The Tribological Properties of Self-Assembled Systems Using Molecular Dynamics

By

Stephanie Alicia Whyte

A thesis submitted to the Graduate Program in the Department of Chemistry

in conformity with the requirements for the

Degree of Master of Science

Queen's University

Kingston, Ontario, Canada

(February, 2015)

Abstract

Static quantum chemical calculations and first principles molecular dynamics simulations are used to examine the behavior of two-dimensional hydrogen-bonded systems under sliding conditions, with the goal of assessing whether such systems may be useful as lubricants. The results demonstrate that these systems can be effective lubricants if the hydrogen bonds (HBs) in the system are of moderate strength, evenly distributed in the system, and restricted to reside within the layers. One system that meets these conditions was found to exhibit friction forces and friction coefficients that are comparable to layered systems consisting of sheets of atoms connected via covalent or ionic bonds, such as graphite and MoS_2. The results also show that the flexibility associated with the HBs allows this system to reversibly undergo large structural deformations. This ability allowed this system to undergo a slip mechanism in which the layers buckled, which was found to reduce the slip barrier. The ability to reversibly accommodate structural changes may represent an advantage of systems comprising sheets of covalently or ionically bonded components, which can be damaged irreversibly as a result of large structural deformations.

Acknowledgements

I would like to acknowledge the following people and organizations for their assistance in the completion of this thesis: my supervisor, Dr. Nicholas Mosey, for giving me the opportunity to work in his group and learn about the field of tribology and tribochemistry while providing continual guidance and encouragement throughout my time at Queen's; all members of the Mosey group who made the learning curve and my time here very enjoyable; Compute Canada, SciNet and Sharcnet for their computational resources; Queen's University, the Department of Chemistry, for financial support; and finally, my amazing family and my wonderful friends for all their help and constant support.

Table of Contents

List of Figures

List of Tables

List of Abbreviations and Symbols

a, **b**, **c:** Lattice vectors of the simulation cell

AFM: Atomic Force Microscopy

DFT: Density Functional Theory

HBs/HB: Hydrogen Bonds/Hydrogen-bonded

FF: Force Fields

FPMD: First-principles Molecular Dynamics

GGA: Generalized Gradient Approximation

HF: Hartree-Fock

KS: Kohn-Sham

LDA: Local Density Approximation

MD: Molecular Dynamics

NVE: Number, Volume and Energy are fixed

PAWs: Projector Augmented Wavefunctions

PBE: Perdew, Burke, Ernzerhoff

PES: Potential Energy Surface

PPs: Pseudopotentials

QC: Quantum Chemical

Δx: Shear distance

$\boldsymbol{\tau}$**:** Shear stress

$\boldsymbol{\mu}$**:** Friction coefficient

L: Normal Load

Chapter 1: Introduction

Friction and wear are phenomena that incur significant economic and environmental costs. For example, it has been estimated that the costs of friction and wear correspond to several percent of the gross domestic products in industrialized nations.[1,2] The economic impact arises from the need to replace prematurely worn equipment, as well as the costs associated with increased energy requirements due to frictional losses. These factors also have environmental impacts, with the replacement of equipment leading to increased waste and frictional losses placing higher demands on energy resources. Lubricants are used to control friction and wear in an effort to reduce these deleterious impacts. The development of improved lubricants would benefit from a better understanding of the fundamental features of friction and wear, as well as the processes that occur within sliding contacts.

The research described in this thesis aims to examine the possibility of using two-dimensional (2D) hydrogen-bonded (HB) systems as robust and effective lubricants. 2D HB networks have been shown to form layered structures similar to those of existing lubricants, such as graphite, molybdenum disulfide (MoS_2), molybdenum trioxide (MoO_3) and boron nitride (BN).[3–6] These systems are effective lubricants because the sheets comprising them interact via van der Waals forces, which allows the sheets[7] to slide past one another with little resistance. However, the covalent or ionic bonds between the components in such sheets are susceptible to irreversible damage under sliding conditions such as oxidation, polymerization, changes in coordination numbers, and decomposition that compromises the ability to retain a layered structure, and hence reduces their abilities as lubricants.[8–16] Meanwhile, the components in 2D HB networks are connected through HBs, which can form and dissociate in a reversible manner, which may render these networks more robust over the long term than analogous systems

composed of covalently or ionically bonded components. As such, 2D HB networks may be effective, long-lasting lubricants. This potential will be explored in this work using chemical simulations of prototypical 2D HB networks.

The remainder of this chapter will introduce concepts that are relevant to this work. A general discussion of friction is provided in Section 1.1, while lubricants are described in Section 1.2. 2D HB networks are described Section 1.3 and computer simulations of friction, wear, and lubrications are described in Section 1.4. Lastly, specific goals of the research are reviewed in Section 1.5.

1.1 Friction

Friction is the force that resists the motion of two materials sliding past one another. Consider, for example, the system in Figure 1.1 in which one block rests upon another. In order to initiate the movement of the upper block relative to the lower block, it is necessary to apply a force, *F*, that is equivalent to the friction force that resists this motion. This force is called the static friction force because it is the friction force associated with the initiation of movement. If the blocks are already in motion, the friction force will resist that motion. The force that must be applied to maintain movement of two surfaces at a constant relative velocity is called the kinetic friction.

Figure 1.1. Two views of surfaces sliding past each other on (a) the macroscopic and (b) the microscopic level.

Friction has been studied for hundreds of years because of its implications throughout many daily activities. The earliest systematic studies of friction are accredited to da Vinci, who examined the forces associated with moving metal plates along surfaces. Similar experiments performed by Amontons led to the basic fundamentals of friction, now known as Amontons' law, which is expressed as:

$$F = \mu L \qquad \text{(Eq. 1.1)}$$

where F is the friction force, L is the normal load (the load acting normal to the interface between the two surfaces in motion) and μ is the friction coefficient. This law suggests that the friction force is zero in the absence of a normal load, does not depend on the cross-sectional area of the surfaces in contact, and does not depend on the relative velocities of these surfaces. Modern research shows that these predictions only hold strictly in the limits of low sliding velocities and in the absence of interactions between the sliding surfaces. However, in most practical cases, Amontons' law is adequate for describing the friction of moving objects. Extensions of Amontons' law have been developed to account for friction under conditions where Eq. 1.1 does not apply.[17–20]

The ability of Amontons' law to accurately account for friction is remarkable considering that this law is based on a macroscopic view of the interactions between sliding surfaces. Specifically, this law is based on the notion that surfaces are perfectly flat and that the apparent contact area between the two surfaces is equivalent to the true contact area. Meanwhile, modern experiments show that surfaces are typically very rough at the microscopic and nanoscopic levels. In particular, surfaces are covered by asperities (microscopic hills) that come into contact with one another when surfaces are brought together, as illustrated in Figure 1.1. The contact area between these asperities corresponds to the true contact area and is typically much lower than the

apparent contact area of the surfaces in contact. The interactions between surfaces at the asperity contacts dictate the friction forces, and thus while friction is typically measured as a macroscopic phenomenon, it has microscopic origins. As such, understanding the behaviour and properties of materials exposed to the conditions achieved at the points of asperity contact is critical to developing a better understanding of friction.

1.2 Lubricants

Although friction is essential for certain applications, such as ensuring tires on cars provide adequate traction, the energy losses and wear associated with friction are detrimental in other scenarios. Lubricants are used to counteract these deleterious effects. In a general sense, a lubricant functions by providing an easily shearable medium that prevents sliding surfaces from coming into contact. The high shearability of lubricants causes slip events to take place with low friction forces and to occur entirely within the lubricant itself. Meanwhile, the ability to keep sliding surfaces from coming into contact allows a lubricant to inhibit wear. This is illustrated in Figure 1.2 where the lubricant is situated between two surfaces sliding past one another. The lubricant reduces the impact between Surface 1 and Surface 2 and because of its chemical layers they can generally slide in both directions in which the surfaces are moving.

Figure 1.2. Basic schematic illustrating how lubricants act as mechanical barriers to lower friction and wear.

Lubricants come in a variety of forms such as synthetic oils,[21] triglycerides,[22] oligomer solutions[23,24] and solid, dry lubricants.[3-6,24] Each type has a unique purpose in industrial applications and can be advantageous in its own way. Solid lubricants such as graphite, MoS_2, and boron nitride have proven to be effective at controlling friction and wear (Figure 1.3).[3–5,25–28] Meanwhile, interlayer interactions are dominated by weak van der Waals forces that lead to low slip barriers, which allow the layers in these systems to slide past one another with low applied forces.

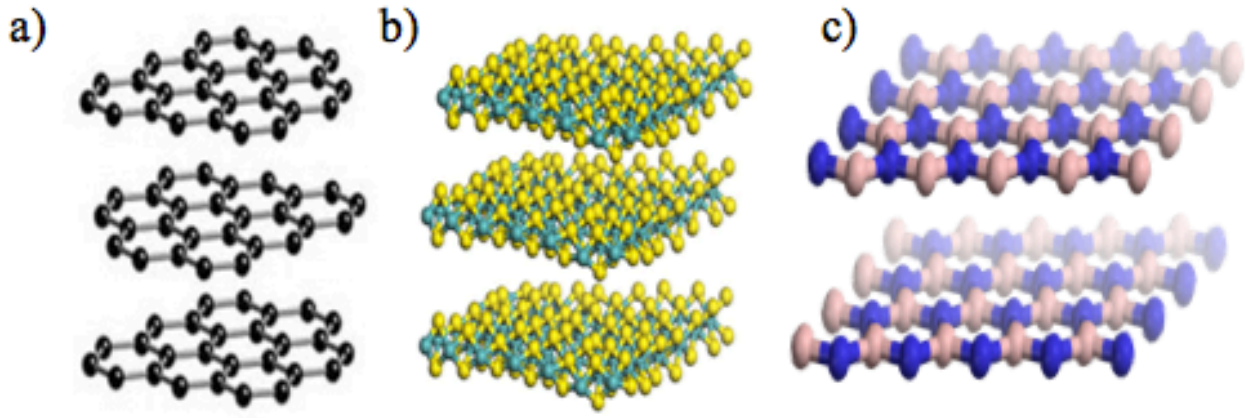

Figure 1.3. Examples of solid, two-dimensional lubricants. Graphite (a)[29], molybdenum disulfide (b)[30] and boron nitride (c)[31] are able to form planar sheets based on a unique arrangement of atoms that create ideal layered structures able to slide past one another easily.

To function as effective lubricants, these systems require the ability to retain layered structures. These structures can be compromised in response to the extreme conditions experience during sliding. As noted above, friction is determined by the interactions between surfaces at points where asperities come into contact during sliding, and thus lubricants must be operational at these contact points. The conditions experienced at these locations are extreme, with peak temperatures approaching the melting points of the materials in contact (e.g. thousands of Kelvin) and stresses reaching the yield strengths of these materials (tens of gigapascals).[32] While the

presence of covalent or ionic bonds between components in the layers of lubricants like those shown in Figure 1.3 offers some resistance to degradation under conditions of extreme temperature and stress, these systems have been observed to undergo irreversible changes in structure that compromise lubricant performance during sliding.[33–37] One of the most well known examples of these changes involves the pressure-induced conversion of graphene into diamond. While this process normally requires exceptionally high pressures, recent studies have demonstrated that placing graphite sheets on a platinum substrate and exposing the uppermost layers to hydrogen can induce a diamond-like structure.[38] This illustrates that the 2D structures of these materials can be altered more easily than once thought possible. MoS_2, as another example, has been shown to lose its effectiveness as a lubricant under various conditions.[39] In one study, MoS_2 was shown to transform into MoO_3 in the presence of oxygen with temperatures nearing 400 K.[40] Similar studies done on MoS_2 prompted researchers to investigate why the oxidation of MoS_2 to MoO_3 causes an increase in wear and friction.[41] Nonetheless, it is evident that although these solid lubricants may be very beneficial under set conditions, they can sometimes become irreversibly disrupted which is not ideal for the process of lubrication.

1.3 Two-dimensional Systems

Experimental work has demonstrated the ability to synthesize materials with one-, two- and three-dimensional architectures composed of species connected through a wide range of interactions. The focus of this research uses the structural properties and fundamental interactions of previously existing 2D systems in order to create ideal systems to act as lubricants. 2D systems have been well studied in the literature and are shown to exist in many different forms making both their industrial and experimental uses very diverse. The directionality and strength of the bonds that make up these systems have a significant impact on their properties and suitability for

various applications. As also mentioned, both the type and subsequently strength of the bond can greatly affect the systems' properties. Some systems are held together by strong covalent or ionic bonds, which yield rigid materials. Other systems are comprised of more flexible interactions allowing them to be used for different applications. A combination of these interactions is what makes graphite, for example, an effective lubricant. Its structure contains both strong intralayer interactions to keep the layers intact along with its weaker interlayer interactions that allows the sheets to move past one another easily.

Hydrogen bonding is another type of interaction that can be present in 2D systems. Hydrogen-bonded systems can be found in areas ranging from biological forms such as DNA to industrial applications like liquid crystal displays. Like any 2D system, the orientation of the bonds can allow the systems to exist in a variety of forms such as planar sheets, crystal structures, bulk systems or small clusters.[42–47] Recent efforts in the area of hydrogen-bonded systems have focused on the abilities of these systems to self-assemble into desired architectures. Self-assembly can be defined as the process in which a disordered system organizes into a specific pattern based on interactions between molecules within the system. This behaviour allows molecular systems to arrange themselves into uniquely ordered structures with little or no external assistance (Figure 1.4). Using hydrogen bonding as a fundamental component in the construction, materials like plastics and polymers have been created that contain the ability to organize themselves into well-defined structures with little to no external assistance.[38,48–51] More importantly, when these materials are deformed, their predetermined interactions allow them to reform to their original arrangement making them very useful in conditions where the materials are commonly exposed to external force. This property of some hydrogen-bonded systems has

been used in the development of self-healing materials, which can reform a desired structure after that structures is disrupted.[51–53]

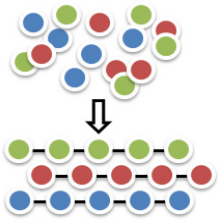

Figure 1.4. Self-organization of molecules into ordered layers.

The focus of this thesis is to examine the lubricating abilities of 2D hydrogen-bonded systems. It is known that 2D systems such as graphite and molybdenum disulfide have been shown to exhibit good lubricating properties due to the fact that they create planar sheets held together via weak van der Waals interactions allowing for them to slide easily past one another. On the other hand, lubricants are exposed to extreme conditions and are therefore susceptible to irreversible damage making them, at times, ineffective. Therefore, creating systems similar to that of graphene but containing hydrogen bonding may create a new class of lubricants whose layers slide easily and are capable of reversible change due to hydrogen bonds between components amongst the layers. Figure 1.5 shows examples of 2D self-assembling systems that take on a variety of different forms.

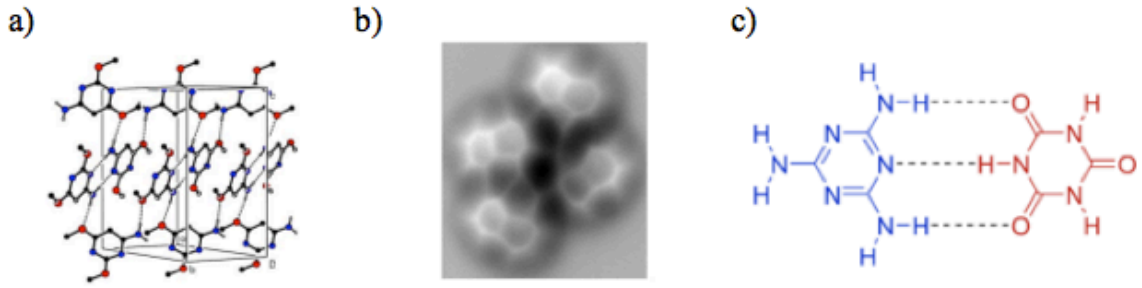

Figure 1.5. Examples of two-dimensional self-assembled systems reported in the literature demonstrating the various stacking arrangements these types of systems may have. (a) shows a layered system where the hydrogen-bonded sheets are reinforced through π-π stacking.[42] (b) contains AFM images of fused rings containing nitrogen and hydroxyl groups connected through hydrogen bonding.[54] (c) illustrates two types of molecules connected via hydrogen bonds to form a unique arrangement.[47,55]

1.4 Theoretical Studies of Friction

As noted above, the research reported in this thesis involves using chemical simulations to test the efficacy of 2D HB systems as lubricants. There are several ways to analyze systems using theoretical and computational methods when experimental work cannot visualize or monitor what is happening at the nanoscopic level. The following section will describe four types of methods and their advantages and disadvantages in the context of this research: phenomenological, finite element, force fields and quantum chemistry. These methods have been proven to be very useful in regards to studying surface structure, friction and the effectiveness of lubricants.

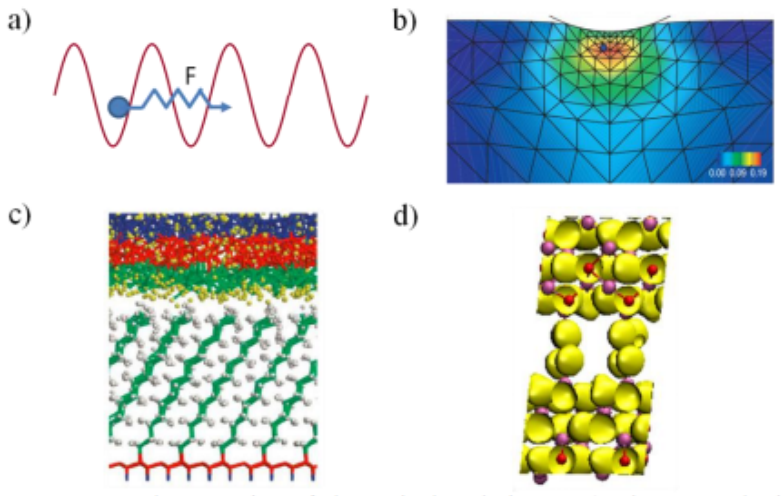

Figure 1.6. Common methods used to capture sliding and friction in various materials. a) represents conceptual methods, where a force is calculated to overcome a potential barrier represented by a sine function. b) the finite element model, where intersecting points based on a grid are used to calculate energies.[56] c) the force field method, where the particle motion is represented by a classical expression[57] and d) the quantum chemical method, where the electron density is used to dictate the motion of atoms.[58]

1.4.1 Conceptual Methods

Early efforts to theoretically understand friction were based on conceptual models. The Prandtl-Tomlinson model is perhaps the most well known of the conceptual models.[59,60] Key features of this model are shown in Figure 1.6(a). Specifically, the potential energy due to interactions between the two sliding surfaces is represented by a sinusoidal function. A mass is placed on this potential energy surface and is attached to a spring with a force constant *k*. The end of the spring can be moved, which exerts a force on the mass and slip occurs when the applied force is equal to the friction force. This model does not capture specific details of a surface, but is useful in the context of determining how friction forces depend on factors such as object masses and potential energy barriers to slip.

1.4.2 Finite Element Models

Finite element models divide a material into a series of domains that are connected via

various parameterized potentials. Friction can then be examined by analyzing the response of the material to applied stresses and strains. In principle, it is possible to resolve the material to the level of individual atoms, but in practice the domains used in finite element models represent microscopic components of a materials. As such, these methods are useful in providing insight into the response of materials to stresses and strains at larger length scales, and are thus used extensively in engineering applications.[61–63] However, finite element calculations resolved to only microscopic length scales do not provide insights into the atomic-level behaviour of chemical systems within sliding contacts.

1.4.3 Force Fields

Force fields (FFs) are used to perform simulations of chemical systems resolved to the level of individual atoms or groups of atoms. FF models relate the energy of a system to its structure using parameterized potential energy functions in conjunction with chemically-intuitive descriptions of geometry. For instance, the geometry of a molecule can be described in terms of bond lengths, bond angles, and torsions, while the changes in energy arising from changes in structure are then described by parameterized functions, e.g. harmonic or Morse potentials to describe the change in energy associated with changing the length of a bond. The use of FFs incurs relatively low computational costs compared to other methods for simulating chemical systems at the atomic level, and can thus be used to study systems containing thousands of atoms over time scales approaching microseconds. As such, FF-based simulations have been used extensively to study the atomic level details of processes occurring in sliding contacts.[64,65] Unfortunately, the functional forms used to describe bonds in most FFs are incapable of describing changes in bonding, which prevents FFs from being used to examine chemical

reactions. Some models that do permit changes in bonding exist;[66,67] however, they require extensive parameterization to be applied in a reliable manner.

1.4.4 Quantum Chemistry

Quantum chemical (QC) methods resolve a chemical system to the level of its electronic structure. The potential energy in such calculations is obtained through an approximate quantum mechanical treatment of the electronic structure. The explicit treatment of the electronic structure allows QC methods to accurately describe changes in bonding. However, computational demands limit QC-based simulations to examining systems containing a few hundred atoms at most over sub-nanosecond time scales. Quantum chemical calculations have been used to investigate the tribological properties (i.e. those associated with friction, wear and lubrication) of solid layered systems.[68–73] Previous studies within the Mosey group have shown that the QC methods have been able to capture such processes with examples like bulk alumina where the system is sheared along a specific direction that give insight into the nanoscopic interactions.[58,74]

This research will use QC methods in conjunction with molecular dynamics (MD) to capture and analyze slip processes with 2D HB networks. Although QC methods can only examine systems containing up to a few hundred atoms over short time scales, their ability to capture changes in bonding and chemical reactions makes them the preferred method for this research because it cannot be assumed that the model systems used in this work do not undergo reactions under sliding conditions. The QC methods used in this research will be discussed in more detail in Section 2.4.

1.5 Goals of Research

This project aims to examine whether 2D HB networks may be useful as lubricants. This will be achieved by performing QC-based MD simulations of model systems containing

components found in experimentally-reported 2D HB networks. The simulations focus on examining the structural changes that occur in response to shear strains and quantifying the energetics and forces associated with slip. The results demonstrate that 2D HB networks may be effective as lubricants if the HBs are moderate in strength and distributed evenly throughout the system. In this case, it is found that these networks can undergo a unique slip mechanism involving large structural changes that leads to lower friction forces. Such a mechanism would not be possible for more rigid systems with layers containing covalent or ionic bonds. Meanwhile, the layered structure is lost through structural reorganization or reactions between components that lead to large friction forces where HBs are not of moderate strength and are not evenly distributed.

The contents of this thesis are organized as follows. Chapter 2 provides an overview of the methods and models used in this work, along with a description of the approaches taken to analyze the results of the simulations. The results are presented in Chapter 3 and include an analysis and discussion of the development of model systems, the behaviour of the model systems under sliding conditions, and detailed quantitative analysis of their corresponding slip processes. Chapter 4 provides conclusions about the results along with potential future work.

---

(1) Persson, B. N. J. Sliding Friction. *Surf. Sci. Rep.* **1999**, *33*, 83–119.

(2) Laboratory, A. N. *Large-Scale Manufacturing of Nanoparticulate-Based Lubrication Additives*; 2009.

(3) Scharf, T. W.; Prasad, S. V. Solid Lubricants: A Review. *J. Mater. Sci.* **2012**, *48*, 511–531.

(4) Cho, M. H.; Ju, J.; Kim, S. J.; Jang, H. Tribological Properties of Solid Lubricants (graphite, Sb_2S_3, MoS_2) for Automotive Brake Friction Materials. *Wear* **2006**, *260*, 855–860.

(5) Wang, J.; Rose, K. C.; Lieber, C. M. Load-Independent Friction : MoO_3 Nanocrystal Lubricants. **1999**, *103*, 8405–8409.

(6) Stefanov, M.; Enyashin, A. N.; Heine, T.; Seifert, G. Nanolubrication : How Do MoS_2 - Based Nanostructures Lubricate ? *J. Phys. Chem. C* **2008**, 112, 17764–17767.

(7) Fox, N. J.; Stachowiak, G. W. Vegetable Oil-Based lubricants—A Review of Oxidation. *Tribol. Int.* **2007**, *40*, 1035–1046.

(8) Qu, J.; Blau, P. J.; Dai, S.; Luo, H.; Meyer, H. M.; Truhan, J. J. Tribological Characteristics of Aluminum Alloys Sliding against Steel Lubricated by Ammonium and Imidazolium Ionic Liquids. *Wear* **2009**, *267*, 1226–1231.

(9) Dascalescu, D.; Polychronopoulou, K.; Polycarpou, A. A. The Significance of Tribochemistry on the Performance of PTFE-Based Coatings in CO_2 Refrigerant Environment. *Surf. Coatings Technol.* **2009**, *204*, 319–329.

(10) Zhang, L.; Feng, D.; Xu, B. Tribological Characteristics of Alkylimidazolium Diethyl Phosphates Ionic Liquids as Lubricants for Steel-Steel Contact. *Tribol. Lett.* **2009**, *34*, 95–101.

(11) Shakhvorostov, D.; Müser, M.; Mosey, N. Correlating Cation Coordination, Stiffness, Phase Transition Pressures, and Smart Materials Behavior in Metal Phosphates. *Phys. Rev. B* **2009**, *79*, 094107.

(12) Mosey, N. J.; Woo, T. K.; Kasrai, M.; Norton, P. R.; Bancroft, G. M.; Müser, M. H. Interpretation of Experiments on ZDDP Anti-Wear Films through Pressure-Induced Cross-Linking. *Tribol. Lett.* **2006**, *24*, 105–114.

(13) Hsu, S. M.; Gates, R. S. Effect of Materials on Tribochemical Reactions between Hydrocarbons and Surfaces. *J. Phys. D. Appl. Phys.* **2006**, *39*, 3128–3137.

(14) Landolt, D. Electrochemical and Materials Aspects of Tribocorrosion Systems. *J. Phys. D. Appl. Phys.* **2006**, *39*, 3128–3137.

(15) Bhushan, B.; Cichomski, M.; Tao, Z.; Tran, N. T.; Ethen, T.; Merton, C.; Jewett, R. E. Nanotribological Charactrization and Lubricant Degradation Studies of Metal-Film Magnetic Tapes Using Novel Lubricants. *J. Tribol.* **2007**, *129*, 621–627.

(16) Hsu, S. M.; Zhang, J.; Yin, Z. The Nature and Origin of Tribochemistry. In *Tribology Letters*; 2002; Vol. 13, pp. 131–139.

(17) Miura, K.; Kamiya, S. Observation of the Amontons-Coulomb Law on the Nanoscale: Frictional Forces between Flakes and Surfaces. *Europhys. Lett.* **2002**, *58*, 610.

(18) Gao, J.; Luedtke, W. D.; Gourdon, D.; Ruths, M.; Israelachvili, J. N.; Landman, U. Frictional Forces and Amontons' Law: From the Molecular to the Macroscopic Scale. *J. Phys. Chem. B* **2004**, *108*, 3410–3425.

(19) Berman, A.; Drummond, C.; Israelachvili, J. Amontons' Law at the Molecular Level. *Tribol. Lett.* **1998**, *4*, 95–101.

(20) Gerde, E.; Marder, M. Friction and Fracture. *Nature* **2001**, *413*, 285–288.

(21) Martins, R.; Seabra, J.; Brito, a.; Seyfert, C.; Luther, R.; Igartua, a. Friction Coefficient in FZG Gears Lubricated with Industrial Gear Oils: Biodegradable Ester vs. Mineral Oil. *Tribol. Int.* **2006**, *39*, 512–521.

(22) Dossat, V.; Combes, D.; Marty, A. Efficient Lipase Catalysed Production of a Lubricant and Surfactant Formulation Using a Continuous Solvent-Free Process. *J. Biotechnol.* **2002**, *97*, 117–124.

(23) Zhu, J.; Liu, W.; Chu, R.; Meng, X. Tribological Properties of Linear Phosphazene Oligomers as Lubricants. *Tribol. Int.* **2007**, *40*, 10–14.

(24) Shubkin, R. L.; Baylerian, M. S.; Maler, A. R. Olefin Oligomer Synthetic Lubricants: Structure and Mechanism of Formation. *Ind. Eng. Chem. Prod. Res. Dev.* **1980**, *19*, 15–19.

(25) Lee, C.-G.; Hwang, Y.-J.; Choi, Y.-M.; Lee, J.-K.; Choi, C.; Oh, J.-M. A Study on The Tribological Characteristics of Graphite Nano Lubricants. *Int. J. Precis. Eng. Manuf.* **2009**, *10*, 85–90.

(26) Saito, T.; Honda, F. Chemical Contribution to Friction Behavior of Sintered Hexagonal Boron Nitride in Water. *Wear* **2000**, *237*, 253–260.

(27) Berman, D.; Erdemir, A.; Sumant, A. V. Reduced Wear and Friction Enabled by Graphene Layers on Sliding Steel Surfaces in Dry Nitrogen. *Carbon N. Y.* **2013**, *59*, 167–175.

(28) Berman, D.; Erdemir, A.; Sumant, A. V. Graphene: A New Emerging Lubricant. *Mater. Today* **2014**, *17*, 31–42.

(29) Darling, D. Encyclopedia of Science: Graphite http://www.daviddarling.info/encyclopedia/G/graphite.html (accessed Jan 8, 2014).

(30) Gao, D. The Macroscopic Level: Friction, Energy Dissipation, and Wear http://www.cmmp.ucl.ac.uk/~kpm/people/dgao.htm (accessed Jan 8, 2014).

(31) Wikipedia. Boron nitride http://en.wikipedia.org/wiki/Boron_nitride#mediaviewer/File:Boron-nitride-(hexagonal)-side-3D-balls.png (accessed Jan 8, 2014).

(32) Jacobson, B.; Hoglund, E. Experimental Investigation of the Shear Strength of Lubricants Subjected to High Pressure and Temperature. *J. Tribol.* **1986**, *108,* 571-577.

(33) Jradi, K.; Schmitt, M.; Bistac, S. Surface Modifications Induced by the Friction of Graphites against Steel. *Appl. Surf. Sci.* **2009**, *255*, 4219–4224.

(34) Savage, R. H. Graphite Lubrication. *J. Appl. Phys.* **1948**, *19*, 1–10.

(35) Sliney, H. E. Solid Lubricant Materials for High Temperatures—a Review. *Tribology International*, 1982, *15*, 305–315.

(36) The Friction of Carbon Fibres. *J. Phys. D. Appl. Phys.* **1976**, *9*, 2517–2532.

(37) Gansheimer, J. A Review on Chemical Reactions of Solid Lubricants During Friction. *ASLE Trans* **1972**, *15*, 244–251.

(38) Rajasekaran, S.; Abild-Pedersen, F.; Ogasawara, H.; Nilsson, A.; Kaya, S. Interlayer Carbon Bond Formation Induced by Hydrogen Adsorption in Few-Layer Supported Graphene. *Phys. Rev. Lett.* **2013**, *111*, 085503.

(39) Zhang, H.-J.; Zhang, Z.-Z.; Guo, F. Studies on the Influence of Graphite and MoS2 on the Tribological Behaviors of Hybrid PTFE/Nomex Fabric Composite. *Tribol. Trans* **2011**, *54*, 417–423.

(40) Wang, J.; Rose, K. C.; Lieber, C. M. Load-Independent Friction: MoO 3 Nanocrystal Lubricants. *J. Phys. Chem. B* **1999**, *103*, 8405–8409.

(41) Windom, B. C.; Sawyer, W. G.; Hahn, D. W. A Raman Spectroscopic Study of MoS2 and MoO3: Applications to Tribological Systems. *Tribology Letters*, 2011, *42*, 301–310.

(42) Glidewell, C.; Low, J. N.; Melguizo, M.; Quesada, A. 4-Amino-2,6-Dimethoxypyrimidine: Hydrogen-Bonded Sheets of R 2 2 (8) and R 6 6 (28) Rings, Reinforced by an Aromatic Π–π-Stacking Interaction. *Acta Crystallogr. Sect. C Cryst. Struct. Commun.* **2003**, *59*, o202–o204.

(43) MacGillivray, L. R. Organic Synthesis in the Solid State via Hydrogen-Bond-Driven Self-Assembly. *J. Org. Chem.* **2008**, *73*, 3311–3317.

(44) Wasio, N. a; Quardokus, R. C.; Forrest, R. P.; Lent, C. S.; Corcelli, S. a; Christie, J. a; Henderson, K. W.; Kandel, S. A. Self-Assembly of Hydrogen-Bonded Two-Dimensional Quasicrystals. *Nature* **2014**, *507*, 86–89.

(45) Bowden, N. Self-Assembly of Mesoscale Objects into Ordered Two-Dimensional Arrays. *Science.* **1997**, *276*, 233–235.

(46) Uemura, S.; Aono, M.; Komatsu, T.; Kunitake, M. Two-Dimensional Self-Assembled Structures of Melamine and Melem at the Aqueous Solution-Au(111) Interface. *Langmuir* **2011**, *27*, 1336–1340.

(47) Prior, T. J.; Armstrong, J. a.; Benoit, D. M.; Marshall, K. L. The Structure of the Melamine–cyanuric Acid Co-Crystal. *CrystEngComm* **2013**, *15*, 5838.

(48) Hager, M. D.; Greil, P.; Leyens, C.; Van Der Zwaag, S.; Schubert, U. S. Self-Healing Materials. *Adv. Mater.* **2010**, *22*, 5424–5430.

(49) Van Gemert, G. M. L.; Peeters, J. W.; Söntjens, S. H. M.; Janssen, H. M.; Bosman, A. W. Self-Healing Supramolecular Polymers in Action. *Macromol. Chem. Phys.* **2012**, *213*, 234–242.

(50) Herbst, F.; Döhler, D.; Michael, P.; Binder, W. H. Self-Healing Polymers via Supramolecular Forces. *Macromol. Rapid Commun.* **2013**, *34*, 203–220.

(51) Wang, R.; Xie, T. Shape Memory- and Hydrogen Bonding-Based Strong Reversible Adhesive System. *Langmuir* **2010**, *26*, 2999–3002.

(52) White, S. R.; Blaiszik, B. J.; Kramer, S. L. B.; Olugebefola, S. C.; Moore, J. S.; Sottos, N. R. Self-Healing Polymers and Composites. *Am. Sci.* **2011**, *99*, 392–399.

(53) Wang, C.; Liu, N.; Allen, R.; Tok, J. B. H.; Wu, Y.; Zhang, F.; Chen, Y.; Bao, Z. A Rapid and Efficient Self-Healing Thermo-Reversible Elastomer Crosslinked with Graphene Oxide. *Adv. Mater.* **2013**, *25*, 5785–5790.

(54) Zhang, J.; Chen, P.; Yuan, B.; Ji, W.; Cheng, Z.; Qiu, X. Real-Space Identification of Intermolecular Bonding with Atomic Force Microscopy. *Science* **2013**, *342*, 611–614.

(55) Wikipedia. Melamine-Cyanurate http://en.wikipedia.org/wiki/Melamine_cyanurate#mediaviewer/File:Melamine-cyanuric_acid_chemical_structure_color.png (accessed Jan 8, 2014).

(56) HAYES, R. L.; HO, G.; ORTIZ, M.; CARTER, E. A. Prediction of Dislocation Nucleation during Nanoindentation of Al3Mg by the Orbital-Free Density Functional Theory Local Quasicontinuum Method. *Philos. Mag.* **2006**, *86*, 2343–2358.

(57) Mikulski, P. T.; Gao, G.; Chateauneuf, G. M.; Harrison, J. A. Contact Forces at the Sliding Interface: Mixed versus Pure Model Alkane Monolayers. *J. Chem. Phys.* **2005**, *122*.

(58) Carkner, C.; Mosey, N. J. Slip Mechanisms of Hydroxylated a-Al2O3 (0001)/(0001) Interfaces: A First-Principles Molecular Dynamics Study. *J. Phys. Chem. C* **2010**, *114*, 17709–17719.

(59) Prandtl, L. Hypothetical Model for the Kinetic Theory of Solid bodies\nEin Gedankenmodell Zur Kinetischen Theorie Der Festen Koerper. *Zeitschrift fur Angew. Math. und Mech.* **1928**, *8*, 85–106.

(60) Tomlinson, G. A. A Molecular Theory of Friction. *Philos. Mag.* **1929**, *7*, 905–939.

(61) Brown, T. D. Finite Element Modeling in Musculoskeletal Biomechanics. *J. Appl. Biomech.* **2004**, *20*, 336–366.

(62) Prendergast, P. J. Finite Element Models in Tissue Mechanics and Orthopaedic Implant Design. *Clinical Biomechanics*, 1997, *12*, 343–366.

(63) Liu, W. K.; Liu, Y.; Farrell, D.; Zhang, L.; Wang, X. S.; Fukui, Y.; Patankar, N.; Zhang, Y.; Bajaj, C.; Lee, J.; et al. Immersed Finite Element Method and Its Applications to Biological Systems. *Comput. Methods Appl. Mech. Eng.* **2006**, *195*, 1722–1749.

(64) Chenoweth, K.; Cheung, S.; Van Duin, A. C. T.; Goddard, W. A.; Kober, E. M. Simulations on the Thermal Decomposition of a Poly(dimethylsiloxane) Polymer Using the ReaxFF Reactive Force Field. *J. Am. Chem. Soc.* **2005**, *127*, 7192–7202.

(65) Galuschko, A.; Spirin, L.; Kreer, T.; Johner, A.; Pastorino, C.; Wittmer, J.; Baschnagel, J. Frictional Forces between Strongly Compressed, Nonentangled Polymer Brushes: Molecular Dynamics Simulations and Scaling Theory. *Langmuir* **2010**, *26*, 6418–6429.

(66) Van Duin, A. C. T.; Dasgupta, S.; Lorant, F.; Goddard, W. A. ReaxFF: A Reactive Force Field for Hydrocarbons. *J. Phys. Chem. A* **2001**, *105*, 9396–9409.

(67) Brenner, D. W.; Shenderova, O. A.; Harrison, J. A.; Stuart, S. J.; Ni, B.; Sinnott, S. B. A Second-Generation Reactive Empirical Bond Order (REBO) Potential Energy Expression for Hydrocarbons. *J. Phys. Condens. Matter* **2002**, *14*, 783–802.

(68) Wang, L. F.; Ma, T. B.; Hu, Y. Z.; Wang, H.; Shao, T. M. Ab Initio Study of the Friction Mechanism of Fluorographene and Graphane. *J. Phys. Chem. C* **2013**, *117*, 12520–12525.

(69) Zartman, G. D.; Liu, H.; Akdim, B.; Pachter, R.; Heinz, H. Nanoscale Tensile, Shear, and Failure Properties of Layered Silicates as a Function of Cation Density and Stress. *J. Phys. Chem. C* **2010**, *114*, 1763–1772.

(70) Koskilinna, J. O.; Linnolahti, M.; Pakkanen, T. . Friction and a Tribochemical Reaction between Ice and Hexagonal Boron Nitride: A Theoretical Study. *Tribol. Lett.* **2008**, *29*, 163–167.

(71) Koskilinna, J. O.; Linnolahti, M.; Pakkanen, T. . Friction Paths for Cubic Boron Nitride: An Ab Initio Study. *Tribol. Lett.* **2007**, *27*, 145–154.

(72) Koskilinna, J. O.; Linnolahti, M.; Pakkanen, T. . Friction Coefficient for Hexagonal Boron Nitride Surfaces from Ab Initio Calculations. *Tribol. Lett.* **2006**, *24*, 37–41.

(73) Liang, T.; Sawyer, W. G.; Perry, S. S.; Sinnott, S. B.; Phillpot, S. R. First-Principles Determination of Static Potential Energy Surfaces for Atomic Friction in MoS_2 and MoO_3. *Phys. Rev. B - Condens. Matter Mater. Phys.* **2008**, *77*.

(74) Haw, S. M.; Mosey, N. J. Chemical Response of Aldehydes to Compression between (0001) Surfaces of -Alumina. *J. Chem. Phys.* **2011**, *134*.

Chapter 2: Methods

This project uses static quantum chemical (QC) calculations and first-principles molecular dynamics (FPMD) to examine the tribological performance of systems consisting of atomically-flat layers that may act as suitable lubricants. These layers are composed of hydrogen-bonded molecules that can be stacked in a manner analogous to that in which graphene sheets are stacked in graphite. To do this, systems representing two-dimensional hydrogen-bonded networks were constructed and placed in simulation cells. The tribological properties of the systems are examined through FPMD simulations when the systems are sheared to induce a slip along specific directions through the deformation of a simulation cell. The direction along which the system was moved was based on the lowest energy slip direction as identified through potential energy surface (PES) scans.

The details of the methods used to perform these calculations are described below. The concept of a simulation cell and periodic boundary conditions is outlined in Section 2.1. The potential energy scan procedure used to identify the directions along which each system was sheared is described in Section 2.2. The molecular dynamics (MD) methods used to perform the simulations are described in Section 2.3 including how the cell is manipulated. The QC methods used in the calculations are described in Section 2.4 and finally, planewave basis sets are discussed in Section 2.5. It should be noted that the development of the model systems are included in Chapter 3.

2.1 Periodic Simulation Cells

Chemical simulations can only be used to study systems containing a finite number of particles, with the QC methods used in this study being applicable to systems

containing a few hundred atoms at most. Meanwhile, the hydrogen-bonded networks of interest to this study consist of extended systems that are much larger than those which can be modeled directly with QC methods. In order to capture the structure of extended systems, it is common practice in QC-based simulations to construct a small system that is representative of the larger system, place the small model in a simulation cell, and then repeat that cell infinitely through the use of periodic boundary conditions. This process is analogous to the manner in which a solid can be described in terms of a periodically repeated unit cell.[1,2]

A simulation cell is defined by three lattice vectors, **a**, **b**, and **c** that point along its edges. In the case of the systems considered in this work, the **a** and **b** vectors are taken to span the *x*-*y* plane and the layers present in the systems will be parallel to this plane. This will facilitate shearing of the system by altering the components of the **c** vector as described in Section 2.3.2.3. The dimensions of the simulation cell, i.e. the lengths of each lattice vector and the angles between them, are selected to accommodate the size of the system that is contained within the cell and provide a realistic representation of the extended system when repeated with periodic boundary conditions.

The concept of a periodically repeated simulation cell is illustrated in Figure 2.1. In this model, the calculation would be performed on the system in the central cell shown. This cell is repeated infinitely in all directions, and the molecules in the central cell interact with the periodic images in the repeated cells. This gives the effect of an extended system. During MD simulations, if one molecule leaves the cell from one side, a periodic image of that molecule enters from the other side. The use of periodic simulation cells is useful in the context of treating extended systems with small

representative models; however, it is important to note that the use of finite size simulation cells prevents the observation of phenomena with length scales greater than that of the simulation cell and the enforced periodic nature of the system may not reflect the actual behaviour of such systems in nature. For instance, the use of periodic boundary conditions in the context of simulating liquids or amorphous systems imposes periodicity that does not exist in the real system.

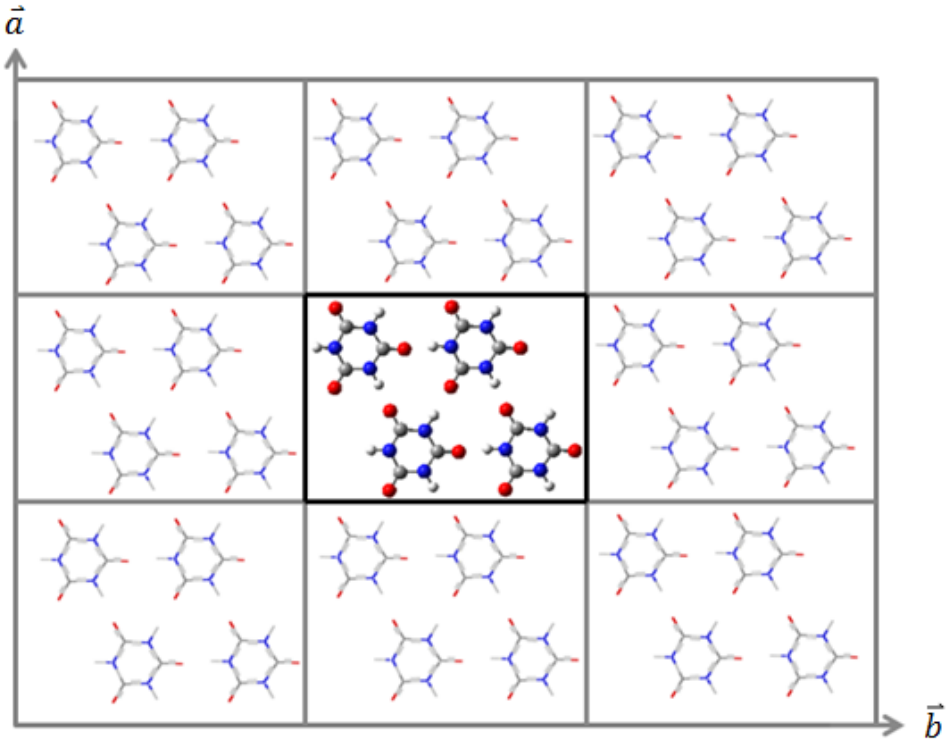

Figure 2.1. Periodic boundary conditions are used to simulate an infinite system. This two-dimensional system is a truncated depiction of the middle "bolded" cell containing four identical molecules being repeated along both the **a** and **b** vector.

2.2 Potential Energy Surface (PES) Scan

In order to evaluate the shear strength of the system, it is necessary to determine the direction along which the system preferentially slips. In layered systems, this will

correspond to the lowest energy pathway along a two-dimensional potential energy surface (PES) associated with moving two neighbouring layers relative to one another. To determine this path, a PES scan was performed in which the upper layer in the simulation cell was moved in fixed increments relative to the lower layer, with the energy evaluated at each increment. The resulting energies then define the PES associated with the movement of one layer past the other, assuming that relaxation effects are not significant. An example of a PES scan produced by this approach is shown in Figure 2.2, where the lowest energy pathway associated with the slip direction is shown by the arrow and the high energy regions (red) are shown along with the low energy regions (blue).

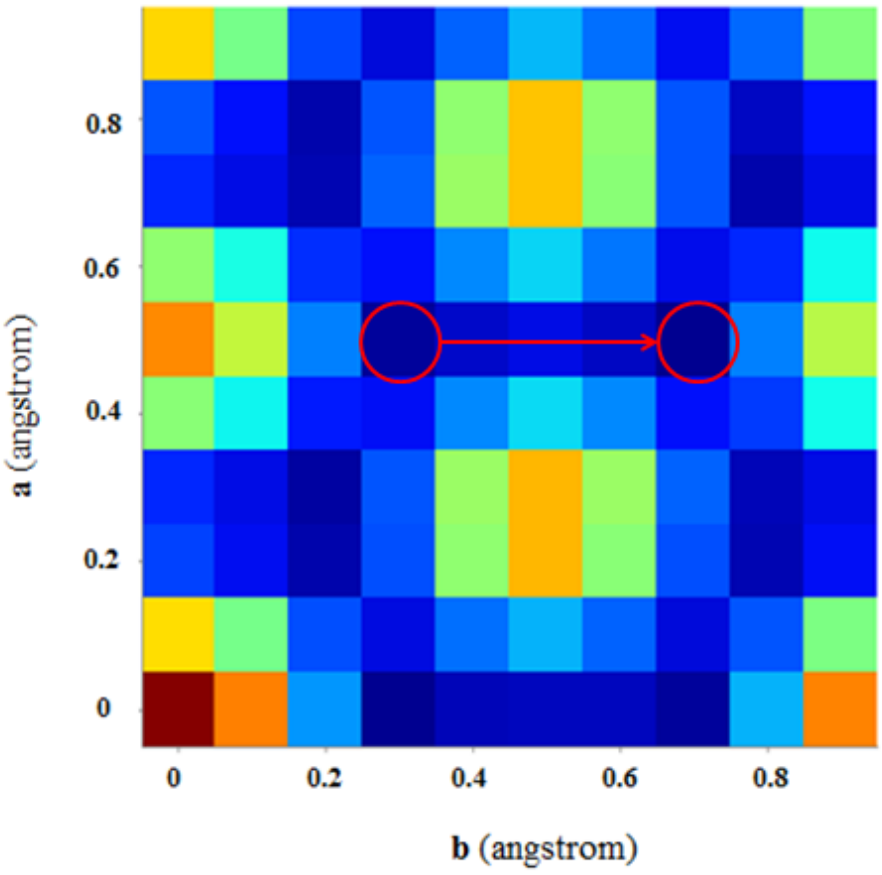

Figure 2.2. PES associated with moving one layer in a layered system relative to a second layer by fixed amounts along the a and b axes. The grid maps out the high (red) and low (blue) energy regions to identify any ideal pathways for shearing. The red circles mark local minima.

2.3 Molecular Dynamics Simulations

Molecular dynamics (MD) simulations were used in this research to study how layered hydrogen-bonded systems respond to shear strains. In MD simulations, the atoms are treated as point masses that move according to Newton's equations of motion. These simulations allow one to study the atomic-level movement of systems exposed to specific external conditions, e.g. temperature and stresses that mimic experiments.[3–6] In addition to gaining qualitative insights into the evolution of chemical systems over time, it is also possible to monitor quantitatively properties that may be difficult to examine experimentally.

In order to perform an MD simulation, one must have a way of evaluating the forces acting on the particles in the system, propagating the positions and velocities of those particles in a manner consistent with Newton's equations, and imposing experimental conditions. Methods for propagating the atoms are described in Section 2.3.1. Techniques for controlling temperature, pressure, and imposing shear are described in Section 2.3.2. The forces used in the MD simulations were evaluated with density functional theory, which is described in Section 2.4.

2.3.1 Propagating Nuclear Positions and Velocities

The basic underlying principle of an MD simulation is to move the atoms in a system over time according to Newton's equations of motion. In practice, the atomic trajectories cannot be evaluated analytically, and thus approximate numerical methods to retrieve updated nuclear positions and velocities are required. In these methods, one must start with the atomic positions and velocities at the present time, *t,* and calculate the forces

acting on the nuclei at that time. These forces are then converted to accelerations using Newton's second law and then this information is used to update the positions and velocities of the nuclei to their values at a slightly later point in time $t + \Delta t$. The period of time over which the system has advanced, Δt, is called the timestep and if the simulation is performed for a total of N steps, then a period of $N\Delta t$ is simulated.

Several algorithms exist for propagating the nuclei over time. The Beeman algorithm[7–9] was used for this purpose in this research because it was the only available integrator that worked in conjuction with variable-cell dynamics (*vide infra*) in the Quantum-Espresso simulation package[10] used to perform the simulations reported in this work. In the Beeman algorithm, the nuclear positions and velocities were propagated according to the following equations:

$$\mathbf{r}(t + \Delta t) = \mathbf{r}(t) + \mathbf{v}(t)\Delta t + \frac{2}{3}\mathbf{a}(t)\Delta t^2 - \frac{1}{6}\mathbf{a}(t - \Delta t)\Delta t^2 \qquad \text{(Eq. 2.1)}$$

$$\mathbf{v}(t + \Delta t) = \mathbf{v}(t) + \frac{1}{6}(2\mathbf{a}(t + \Delta t)) + 5\mathbf{a}(t) - \mathbf{a}(t - \Delta t)\,\Delta t \qquad \text{(Eq. 2.2)}$$

where **r**, **v**, and **a** indicate a nuclear position, velocity, and acceleration, respectively.

The timestep is a key variable in determining the quality of an MD simulation. In particular, the timestep must be chosen to be sufficiently short in order to accurately describe the highest frequency motion in the system, which usually corresponds to the vibrations of bonds containing hydrogen atoms that have oscillation periods of ~10^{-14} s.[11] Thus, one would like to use a small value of Δt to properly integrate the nuclear trajectories. However, the use of a shorter timestep will require a greater number of MD simulation steps to be performed to simulate a given period of time, and thus from a computational standpoint, one would like to use large values of Δt. Ultimately, the goals of accuracy and cost are balanced by selecting the largest value of Δt that accurately

captures the underlying movement of the atoms, which is reflected in the conservation of the total energy of the system. In this study, a value of Δt = 1.0 fs was used, which was found to conserve the total energy of the system to 1.0×10^{-5} au/ps or better.

2.3.2 Imposing external conditions

Computational chemistry allows one to study the atomic-level details of chemical systems that may be difficult to obtain experimentally. In order for this information to be relevant to experiments and other practical applications, it is important to ensure that the simulated conditions are representative of what is encountered in real-world scenarios. In the context of this study, it is important to consider means of controlling the temperature and pressure of the system, as well as imposing shear strains because it is understood lubricants are usually exposed to these external conditions. The approaches taken to do this are discussed below.

2.3.2.1 Controlling Temperature

The temperature of a system is a measure of its kinetic energy and is thus directly related to the nuclear velocities. As such, controlling the velocities of the atoms in the system is key to controlling the system's temperature during an MD simulation. A variety of techniques exist for controlling nuclear velocities during the simulations.[12–14] In this study, the thermostat developed by Andersen was used to control the temperature of the system.[15] The Andersen thermostat is a stochastic thermostat that aims to mimic the transfer of energy between atoms and/or molecules via random collisions.[15,16] To do this, an atom(s) is selected via a random process and its velocity is reassigned to a value selected randomly from a Maxwell-Boltzmann distribution at the desired temperature. In practice, one defines a collision frequency, ν, which indicates how frequently the atomic

velocities will be reassigned. At each MD step, a random number, *R,* is selected for each atom in the system and if $R < \nu\Delta t$ (where Δt is the decided time step), the velocity of the atom is reset. This stochastic approach formally samples the canonical ensemble. However, the random manner in which the velocities are reassigned disrupts the true dynamics of the system. Alternative approaches that are not stochastic, e.g. Nose-Hoover thermostats[17,18], exist, but are not available in the Quantum-Espresso code in conjunction with the variable cell dynamics methods used in the simulations. In practice, the use of a stochastic thermostat is of little consequence to the simulations performed in this work due to the fact that the thermostat is only used to equilibrate the system. It is removed during the portion of the simulation where the system is sheared to avoid suppressing any shear-induced changes in temperature.

2.3.2.2 Controlling Pressure

The study of friction typically involves examining the behavior of a system that is sheared in the presence of an external load, which is introduced in the form of pressure, *P*. To maintain the pressure, it is common practice to employ variable-cell dynamics methods in which the lattice vector representing the cell are treated as dynamic variables that move over time to maintain the desired pressure. In this work, variable-cell dynamics were performed according to the method of Parrinello and Rahman.[19] This technique performs the dynamics using an extended Lagrangian of the form:

$$L = \frac{1}{2}\sum m_{\mathrm{i}}\, \mathbf{s_i^T G s_i} + V(\mathbf{r}) + \frac{1}{2} W \mathrm{Tr}(\mathbf{h^T \cdot h}) - (P - P_{ext})\Omega \qquad \text{(Eq.2.3)}$$

where **h** is a matrix containing the lattice vectors as columns, **r** represents the positions of the atoms in Cartesian coordinates, **s** represents the positions of the atoms as fractional

coordinates of the lattice vectors, i.e. $\mathbf{r} = \mathbf{hs}$, $G = \mathbf{h}^T\mathbf{h}$ is the metric tensor, m_i is the mass of atom i, W is a fictitious mass assigned to the lattice vectors, $V(\mathbf{r})$ is the potential energy, P represents the instantaneous internal pressure of the system, P_{ext} represents the target external pressure and Ω is the volume of the simulation cell.

In practice, the Parrinello-Rahman approach treats the lattice vectors as three extra particles in the system, which have artificially assigned masses and move according to Newtonian dynamics. The forces act on the lattice vectors that correspond to the differences between the external and internal pressures. In the context of the simulations reported below, the movement of the lattice vectors was restricted so that only the *z* component of the **c** lattice vector could change to maintain the desired normal pressure while all other components of the lattice vectors were either fixed or deformed to impose the desired shear strain.

2.3.2.3 Applying Strain

In the context of studying lubrication, it is necessary to model conditions in which the components of the system slide past one another. In this study, this was achieved by shearing the simulation cell along the slip direction by altering the *x* and *y* components of the **c** lattice vector at fixed velocities. This concept is illustrated on the right side of Figure 2.3, which shows how the initial cell (in the center of Figure 2.3) is deformed by moving the **c** vector along the slip direction at a velocity of δ_{rate}. This process causes the upper portion of the simulation cell to move relative to the lower portion, which ultimately leads to a portion of the system moving past another during the slip event. As indicated in Figure 2.3, the system can be sheared in this manner while maintaining a constant normal pressure using the Parrinello-Rahman method described above.[19] It

would be ideal to shear the system at velocities similar to those in realistic conditions, which are on the order of 1.0 m/s or slower. However, such slow rates are not accessible in the MD simulations reported here due to computational expense. Therefore, the systems were sheared at a rate of 1.0 Å/ps (100 m/s) in order to achieve a "complete" simulation (past the point of slip) in approximately two weeks of simulation time. Tests at slower shear rates of 0.5 Å/ps and 0.2 Å/ps showed that the calculated properties are insensitive to this parameter.

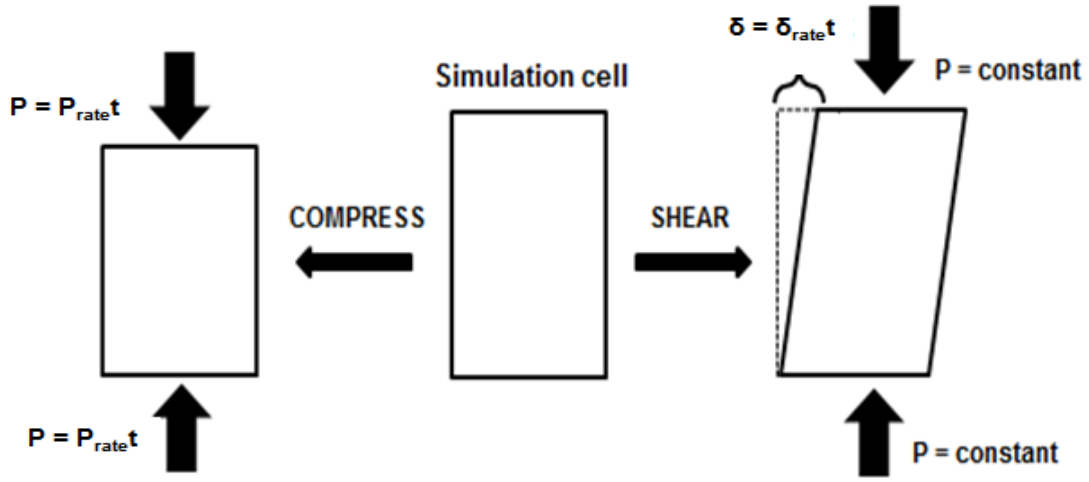

Figure 2.3. Manipulation of a simulation cell (middle) to apply compressive loads (left) or shear strains (right). P indicates the external normal pressure, P_{rate} is the rate at which P is changed, δ is the distance the system has been sheared along the slip direction, and δ_{rate} is the rate of shear.

Shearing the cell effectively corresponds to subjecting the system to an external shear stress. This stress is balanced by the internal stresses of the system, which can be monitored during the simulation. A typical representation of the change in the shear stress, σ, as a function of time is shown in Figure 2.4. The data show that the stress increases in an approximately linear manner before dropping significantly. The drop is

due to a slip event and the value of σ at this point corresponds to the shear strength of the material. This quantity is directly related to the friction force, $F = \sigma A$, where A is the cross-sectional area of the system, and is a key quantity that can be obtained in these calculations. Obtaining F at different normal loads, L, allows one to obtain the friction coefficient, which is the slope of the F-L relationship. The ability to impose different loads is achieved by compressing the system to a desired normal pressure at a constant rate, as indicated on the left side of Figure 2.3, and then maintaining that normal pressure with Parrinello-Rahman methods.

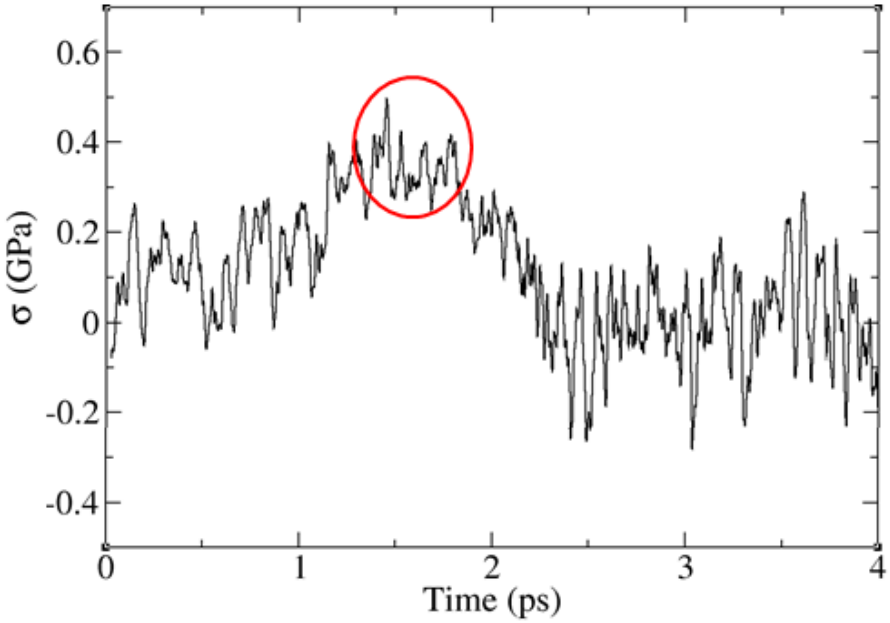

Figure 2.4. Generic representation of a shear stress plot as a function of time. The slip indicated at approximately 1.6 ps is identified as a sharp peak circled in red followed by a sudden decrease. This pattern is seen in most standard simulations of shear although in some cases the slip is not as dramatic.

2.4 Quantum Chemistry

Quantum chemical (QC) methods describe a chemical system down to the level of the electronic structure. These calculations are useful in the context of examining

chemical reactions because they can capture the changes in electronic structure that occur during the formation and dissociation of chemical bonds.[20–22] In practice, it is not possible to treat the electronic structure of a molecule in an exact manner. As such, numerous methods have been developed to obtain an approximate description of the electronic structure. These methods use various approximations, which affect accuracy and the computational requirements for the calculations. In a broad sense, QC methods can be divided into two categories: wavefunction methods and density functional theory. Wavefunction methods attempt to solve the electronic Schrodinger equation, and include techniques like Hartree-Fock (HF), Moller-Plesset (MPn) perturbation theory, coupled-cluster (CC) calculations and configuration interaction (CI) calculations. Hartree-Fock calculations incur low computational demands, permitting calculations of systems containing up to a few hundred atoms, but often result in large errors when compared to experiments. Methods such MPn, CC, and CI calculations provide improved accuracy, but the computational demands of these methods limits their application to relatively small systems. Density functional theory (DFT) aims to treat the electron density as the basic variable for describing the electronic structure. DFT methods typically incur costs that are comparable to Hartree-Fock calculations, yet provide results that generally have much better agreement with experimental data. As such, DFT has become the dominant QC method in recent years. In the present study, the energies and forces used in the FPMD simulations and PES scans were obtained through DFT calculations using planewave basis sets in conjunction with pseudopotentials. General overviews of DFT, planewave basis sets and pseudopotentials are described in what follows.

2.4.1 Density Functional Theory

DFT methods attempt to describe the electronic structure of a molecule in terms of its electron density. Its appeal is reflected not only in the accuracy it offers but also because of its efficiency in comparison to other methods. The main concept behind DFT is to use the electron density of a system to retrieve all components of the Hamiltonian. If all parts of the Hamiltonian operator can be obtained from the density then the ground state and excited states of a system can be determined. This ability was first proven by Hohenberg and Kohn[23], who showed that there is a definite relation between the ground state energy of a many-electron system and the ground state electron density. This relationship can be shown in the form of a functional as shown below:

$$E[\rho] = T[\rho] + E_{Ne}[\rho] + E_{ee}[\rho] \qquad \text{(Eq. 2.4)}$$

where ρ represents the electron density which is a function of the spatial coordinates of the system. A functional, such as T[ρ], allows one to calculate a property, for example the kinetic energy, if one is given the density, ρ. T[ρ] is the kinetic energy of the electrons, $E_{Ne}[\rho]$ is the nuclear-electron interaction energy and $E_{ee}[\rho]$ is the electron-electron interaction energy. Further adaption of this model resulted in the very successful Kohn-Sham model[24], which uses a set of one-electron orbitals, χ, to represent the electronic structure. These orbitals are eigenfunctions of the Kohn-Sham operator and are optimized minimize the energy of the system. Unlike Hartree-Fock, the Kohn-Sham orbitals contain no physical meaning and are simply employed as a convenient means of constructing a reference electronic structure that can be used to obtain the electron density of the real system.[24,25] The density is retrieved from the orbitals by evaluating:

$$\rho(\mathbf{r}) = \sum_{i=1}^{N} \chi_i^*(\mathbf{r})\chi_i(\mathbf{r}) \qquad \text{(Eq. 2.5)}$$

and then the combination of both the orbitals and density can be used in conjunction with the Kohn-Sham energy functional:[24]

$$E[\rho] = \sum_{i=1}^{N} \int \chi_i^*(\mathbf{r}) \left(-\frac{\nabla_i^2}{2} \right) \chi_i(\mathbf{r}) d\mathbf{r} + \sum_{I=1}^{M} \int \frac{Z_I \rho(\mathbf{r})}{|\mathbf{r} - \mathbf{R}_I|} d\mathbf{r} + \frac{1}{2} \sum_{i=1}^{N} \iint \frac{\rho(\mathbf{r}_1)\rho(\mathbf{r}_2)}{|\mathbf{r}_1 - \mathbf{r2}|} d\mathbf{r}_1 d\mathbf{r}_2 + E_{xc}[\rho] \quad \text{(Eq. 2.6)}$$

to obtain the electronic energy. This is used as the potential energy in the FPMD simulations used in this study. Differentiating this energy with respect to the nuclear positions yields the forces on the nuclei used in the simulations.

The first term in the Kohn-Sham energy functional accounts for the kinetic energy of the reference system of the Kohn-Sham orbitals. It should be noted that this is not the exact kinetic energy for the real system. The second term accounts for the nuclear-electron Coulomb interaction energy. The third term represents the Coloumb repulsion due to each electron moving in the average electric field of other electrons in the system.

The final term in the Kohn-Sham functional is known as the exchange-correlation functional and is the only term in the Kohn-Sham equations whose form is not exactly known and therefore must be approximated. This term, in principle, accounts for all contributions to the energy that are not captured by the other terms in the energy functional; the exchange energy arising from Pauli repulsion between electrons, the electron correlation energy that accounts for instantaneous Coulomb interaction, a correction for self-interaction energy that originates from an electron interacting with itself, and a correction corresponding to differences between the kinetic energies of the reference system and the real system.

The accuracy of the KS-DFT relies heavily on the exchange-correlation functional, $E_{xc}[\rho]$, because this is the only term in the Kohn-Sham energy functional that must be approximated. A wide range of approximations for $E_{xc}[\rho]$ exist, with different levels of approximation employing different pieces of information. The most basic approximation is known as the local density approximation (LDA)[26], which yields exchange-correlation functionals that rely solely on the density. Such functionals are often suitable for metals[27,28], where the electron density varies slowly, but do not describe molecular systems in a very accurate manner. Generalized gradient approximation (GGA) functionals build upon LDA functionals by using information regarding the gradient of the electron density in addition to the density itself. These functionals are better able to describe the rapidly varying changes in electron density found in molecules and are thus suitable for studying chemical processes. Additional functionals build on the GGA by adding higher-order derivatives of the density and/or incorporating Hartree-Fock exchange.[29] Such methods can be quite accurate but due to computational expense are not adaptable to DFT calculations employing planewave basis sets like those performed in this study. As such, this work uses the PBE functional, which is of the GGA type.[30] This functional has been shown to provide reasonable reaction energetics and hydrogen bonding.[31,32] However, GGA functionals do not describe dispersion interactions properly and such interactions are important for the systems considered in this study. Therefore, the PBE functional is augmented with the dispersion corrections introduced by Grimme.[33,34]

2.5 Planewave DFT

The Kohn-Sham DFT (KS-DFT) orbitals are typically expressed as linear combinations of basis functions:[24]

$$\chi(\mathbf{r}) = \sum_{v=1}^{K} c_{vi}\, \phi_v(\mathbf{r}) \qquad \text{(Eq. 2.7)}$$

where χ is the Kohn-Sham molecular orbital, K is the total number of basis functions, v is the index of the basis function, c_{vi} is the mixing coefficient and ϕ_v is the basis function. The mixing coefficient in this equation is optimized to yield the most suitable wavefunction for the system.

The two most common types of basis sets used in QC calculations are localized, atom-centred functions and plane waves. In this work, planewave basis functions were used. These functions are expressed as follows:[35,36]

$$\boldsymbol{\phi}_{\mathrm{PW}}(\mathbf{r}) = \frac{1}{\sqrt{\Omega}} e^{i\mathbf{G}\cdot\mathbf{r}} \qquad \text{(Eq. 2.8)}$$

where Ω represents the volume of the simulation cell and $\mathbf{G}$ is the wave vector of the planewave defined by the reciprocal lattice vectors of the unit cell.

Planewave basis sets are common where periodic boundary conditions are used due to the fact that they have the same periodicity as the simulation cell containing the system. This is important because it ensures the electronic structure of the system has the correct periodicity. In addition, unlike localized basis sets, these functions are not centered on specific nuclei meaning all regions of space are treated equally. These functions are also mathematically convenient because they are orthonormal and permit the evaluation of quantities in either real-space or reciprocal spaces, with the transformation between these spaces being facilitated by fast Fourier transforms. This is

particularly advantageous due to the fact that some calculations are much faster in one space than in the other. For example, the construction of the electron density from the orbitals, is represented as N^2 in real space whereas it would be represented in Nlog(N) in reciprocal space.

A significant disadvantage of using plane waves stems from the fact that they do not generally reflect the shapes of electronic state. This is particularly true in the case of the core states for atoms, which have high curvature.[37] In order to capture the curvature of these states properly, it is necessary to employ planewave basis functions with very high frequencies, which in turn requires that of Eq. 2.8 to include a tremendous number of planewaves and makes the calculations intractable. As such, it is common practice to replace the core electrons in planewave DFT calculations with pseudopotentials (PPs) that account for the interactions between the core and valence electrons without employing an explicit representation of the core electrons.[38] The replacement of the core electrons by PPs generally has a minimal effect on the calculation of chemical properties, since core electrons play little role in bonding. However, the use of PPs allows one to dramatically reduce the size of the planewave basis set used in the calculation. In this study, the core electrons were replaced by projector augmented wavefunctions (PAWs), which are a form of PPs that permits the use of very low cutoffs while providing the ability to recover an approximation to the core electron density if necessary.[39]

---

(1) Makov, G.; Payne, M. Periodic Boundary Conditions in Ab Initio Calculations. *Phys. Rev. B* **1995**, *51*, 4014–4022.

(2) Allen, M. Introduction to Molecular Dynamics Simulation. *Comput. Soft Matter From Synth. Polym. to Proteins* **2004**, *23*, 1–28.

(3) Remington, B. A.; Allen, P.; Bringa, E. M.; Hawreliak, J.; Ho, D.; Lorenz, K. T.; Lorenzana, H.; McNaney, J. M.; Meyers, M. A.; Pollaine, S. W.; et al. Material Dynamics under Extreme Conditions of Pressure and Strain Rate. *Mater. Sci. Technol.* **2006**, *22*, 474–488.

(4) Remington, B. A.; Bazan, G.; Belak, J.; Bringa, E.; Colvin, J. D.; Edwards, M. J.; Glendinning, S. G.; Kalantar, D. H.; Kumar, M.; Lasinski, B. F.; et al. Materials Science under Extreme Conditions of Pressure and Strain Rate. *Metall. Mater. Trans. A* **2004**, *35*, 2587–2607.

(5) Hooper, J. B.; Bedrov, D.; Smith, G. D.; Hanson, B.; Borodin, O.; Dattelbaum, D. M.; Kober, E. M. A Molecular Dynamics Simulation Study of the Pressure-Volume-Temperature Behavior of Polymers under High Pressure. *J. Chem. Phys.* **2009**, *130*, 144904.

(6) Desgranges, C.; Delhommelle, J. Viscosity of Liquid Iron under High Pressure and High Temperature: Equilibrium and Nonequilibrium Molecular Dynamics Simulation Studies. *Phys. Rev. B - Condens. Matter Mater. Phys.* **2007**, *76*.

(7) Beeman, D. Some Multistep Methods for Use in Molecular Dynamics Calculations. *J. Comput. Phys.* **1976**, *20*, 130–139.

(8) Verlet, L. Computer "Experiments" on Classical Fluids. II. Equilibrium Correlation Functions. *Phys. Rev.* **1968**, *165*, 201–214.

(9) Schofield, P. Computer Simulation Studies of the Liquid State. *Computer Physics Communications*, 1973, *5*, 17–23.

(10) Giannozzi, P.; Baroni, S.; Bonini, N.; Calandra, M.; Car, R.; Cavazzoni, C.; Ceresoli, D.; Chiarotti, G. L.; Cococcioni, M.; Dabo, I.; et al. QUANTUM ESPRESSO: A Modular and Open-Source Software Project for Quantum Simulations of Materials. *J. Phys. Condens. Matter* **2009**, *21*, 395502.

(11) Kolesov, B. A.; Geiger, C. A. Behavior of H2O Molecules in the Channels of Natrolite and Scolecite: A Raman and IR Spectroscopic Investigation of Hydrous Microporous Silicates. *Am. Mineral.* **2006**, *91*, 1039–1048.

(12) Hoover, W. G. Nose-Hoover Nonequilibrium Dynamics and Statistical Mechanics. *Mol. Simul.* **2007**, *33*, 13–19.

(13) Martyna, G. J.; Klein, M. L.; Tuckerman, M. Nose-Hoover Chains:the Canonical Ensemble via Continuous Dynamics. *J. Phys. Chem.* **1992,** *4,* 2365-2643.

(14) Berendsen, H. J. C.; Postma, J. P. M.; van Gunsteren, W. F.; DiNola, A.; Haak, J. R. Molecular Dynamics with Coupling to an External Bath. *J. Chem. Phys.* **1984**, *81*, 3684–3690.

(15) Andersen, H. . Molecular Dynamics Simulations at Constant Pressure And/or Temperature. *J. Chem. Phys.* **1980**, *72*, 2384–2393.

(16) E, W.; Li, D. The Andersen Thermostat in Molecular Dynamics. *Commun. Pure Appl. Math.* **2008**, *61*, 96–136.

(17) Nose, S.; Nosé, S.; Nosé, S. A Unified Formulation of the Constant Temperature Molecular Dynamics Methods. *J. Chem. Phys.* **1984**, *81*, 511–519.

(18) Hoover, W. G. Canonical Dynamics: Equilibrium Phase-Space Distributions. *Phys. Rev. A* **1985**, *31*, 1695–1697.

(19) Parrinello, M.; Rahman, A.; Parrinello M, R. A. Crystal Structure and Pair Potentials: A Molecular Dynamics Study. *Phys. Rev. Lett.* **1980**, *45*, 1196–1199.

(20) Clary, D. C. Quantum Dynamics of Chemical Reactions. *Science.* **2008**, *321*, 789–791.

(21) Cukier, R. I. Quantum Molecular Dynamics Simulation of Proton Transfer in Cytochrome c Oxidase. *Biochim. Biophys. Acta* **2004**, *1656*, 189–202.

(22) Ahmed, F.; Miura, R.; Hatakeyama, N.; Takaba, H.; Miyamoto, A.; Salahub, D. R. Quantum Chemical Molecular Dynamics Study of the Water–Gas Shift Reaction on a Pd/MgO(100) Catalyst Surface. *J. Phys. Chem. C* **2013**, *117*, 5051–5066.

(23) Hohenberg, P.; Kohn, W. Inhomogeneous Electron Gas. *Phys. Rev.* **1964**, *136*, B864–B871.

(24) Kohn, W.; Sham, L. J. Self-Consistent Equations Including Exchange and Correlation Effects. *Phys. Rev.* **1965**, *140*.

(25) Stowasser, R.; Hoffmann, R. What Do the Kohn-Sham Orbitals and Eigenvalues Mean? *J. Am. Chem. Soc.* **1999**, *121*, 3414–3420.

(26) Perdew, J. P. Density-Functional Approximation for the Correlation Energy of the Inhomogeneous Electron Gas. *Phys. Rev. B* **1986**, *33*, 8822–8824.

(27) Stampfl, C.; Van de Walle, C. Density-Functional Calculations for III-V Nitrides Using the Local-Density Approximation and the Generalized Gradient Approximation. *Phys. Rev. B* **1999**, *59*, 5521–5535.

(28) Arai, M.; Fujiwara, T. Electronic Structures of Transition-Metal Mono-Oxides in the Self-Interaction-Corrected Local-Spin-Density Approximation. *Phys. Rev. B* **1995**, *51*, 1477–1489.

(29) Iikura, H.; Tsuneda, T.; Yanai, T.; Hirao, K. A Long-Range Correction Scheme for Generalized-Gradient-Approximation Exchange Functionals. *J. Chem. Phys.* **2001**, *115*, 3540–3544.

(30) Perdew, J.; Burke, K.; Ernzerhof, M. Generalized Gradient Approximation Made Simple. *Phys. Rev. Lett.* **1996**, *77*, 3865–3868.

(31) Ireta, J.; Neugebauer, J.; Scheffler, M. On the Accuracy of DFT for Describing Hydrogen Bonds: Dependence on the Bond Directionality. *J. Phys. Chem. A* **2004**, *108*, 5692–5698.

(32) Grimme, S. Semiempirical GGA-Type Density Functional Constructed with a Long-Range Dispersion Correction. *J. Comput. Chem.* **2006**, *27*, 1787–1799.

(33) Grimme, S.; Antony, J.; Schwabe, T.; Mück-Lichtenfeld, C. Density Functional Theory with Dispersion Corrections for Supramolecular Structures, Aggregates, and Complexes of (bio)organic Molecules. *Org. Biomol. Chem.* **2007**, *5*, 741–758.

(34) Grimme, S.; Antony, J.; Ehrlich, S.; Krieg, H. A Consistent and Accurate Ab Initio Parametrization of Density Functional Dispersion Correction (DFT-D) for the 94 Elements H-Pu. *J. Chem. Phys.* **2010**, *132*, 154104.

(35) Nichols, P.; Govind, N.; Bylaska, E. J.; De Jong, W. A. Gaussian Basis Set and Planewave Relativistic Spin-Orbit Methods in NWChem. *J. Chem. Theory Comput.* **2009**, *5*, 491–499.

(36) Ambrosch-Draxl, C. Augmented Planewave Methods. *Phys. Scr.* **2004**, *T109*, 48.

(37) Troullier, N.; Martins, J. L. Efficient Pseudopotentials for Plane-Wave Calculations. II. Operators for Fast Iterative Diagonalization. *Phys. Rev. B* **1991**, *43*, 8861–8869.

(38) Schwerdtfeger, P. The Pseudopotential Approximation in Electronic Structure Theory. *ChemPhysChem* **2011**, *12*, 3143–3155.

(39) Blöchl, P. E. Projector Augmented-Wave Method. *Phys. Rev. B* **1994**, *50*, 17953–17979.

Chapter 3: Results and Discussion*

The goal of this thesis is to use chemical simulations to assess whether two-dimensional (2D) hydrogen-bonded (HB) systems may be useful as lubricants. In order to perform the simulations it was necessary to construct model systems. The details of the model development process are described in Section 3.1 and the details of the chemical simulations are reported in Section 3.2. The calculations involved use geometry optimizations, potential energy surface scans and molecular dynamics simulations to assess the structural features of the model systems, to identify the directions along which slip occurs, to explore the atomic-level features associated with the slip processes and to evaluate the associated friction forces.

The structural features and binding energetics of the systems considered in the calculations are reported in Section 3.3. The results of MD simulations performed in the absence of an external load are reported in Section 3.4. These simulations show that the systems examined in this study exhibit a wide range of behaviors when sheared, including reactions between layers, reorganization to lose its layered structure, and the retention of a layered structure throughout the slip process. The details of the processes are explored in detail and related to the electronic structures and orientations of the HBs in the system. The system that retains a layered structure was found to exhibit low friction and was examined further through MD simulations performed at non-zero loads. The results of these simulations are reported in Section 3.5 and show that this system possesses a low friction coefficient and undergoes a load-dependent slip mechanism. At low loads, this system undergoes a slip mechanism in which the layers buckle in a manner that lowers the slip barrier, whereas the layers remain flat during slip at higher loads. The recovery of the layered structure after undergoing the buckled slip mechanism at low loads illustrates the robust nature of 2D HB systems. Overall, the results

indicated that these kinds of systems may be effective lubricants if the HBs are of moderate strength and reside entirely within the layers. These insights may be useful in the development of these types of lubricants for practical applications.

3.1. Development of Model Systems

The experimental development and characterization of 2D hydrogen-bonded networks has been reported in the literature;[1–3] however, many of these systems are too large to study with the FPMD simulation methods used in this work. In particular, the computational demands of these methods limit the systems that could be examined in a reasonable timeframe, e.g. approximately two weeks of simulation time to obtain the shear strength of one system at a given load, to systems containing approximately one hundred atoms or less. As such, small model systems were developed that contained components found in existing 2D hydrogen-bonded networks.[4] In addition, experimentally reported 2D hydrogen-bonded networks can possess a variety of morphologies with some existing as layered structures with no hydrogen bonds (HBs) between layers[3,5,6] and others possessing interlayer HBs.[1] Simulations show that the presence of HBs between sliding interfaces leads to increased shear strengths and friction coefficients.[7,8] As such, the models considered in the calculations were constructed to adopt structures in which the molecules comprising each layer were connected via HBs, yet no interlayer HBs exist.

The components considered for incorporation into the model systems include rings, which encourage the formation of layered structures, and species such as oxygen and nitrogen atoms, and OH, NH, NH_2 groups that can act as HB donors and acceptors to connect the molecular components within the layers. Two different approaches to model design were

employed and are described below. These approaches to model development indicate that the three systems shown in Figure 3.1 exhibit the desired properties of forming stacked atomically-flat hydrogen-bonded layers. The abilities of these systems to form layered structures were assessed through geometry optimizations of model systems that were initially configured in a layered arrangement. It is assumed that the presence of surfaces in sliding contacts would provide a driving force that would encourage the formation of layers parallel to these surfaces.[9]

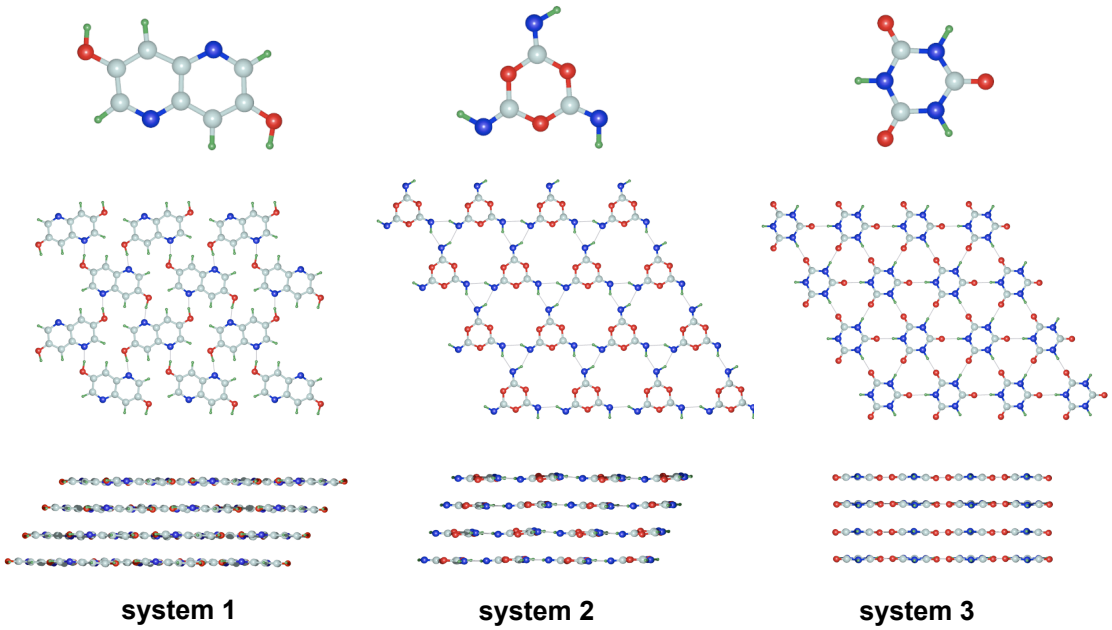

Figure 3.1. Structures of Systems **1**, **2**, and **3** comprised using method I (**1**) and II (**2**,**3**). In each case, the upper panel shows the molecular species on which each system is based, the middle panel shows a top view of a single layer of each system, and the bottom panel shows a side view of each system to illustrate the layered structure. To aid in visualizing the extended structures, each simulation cell has been replicated. The top and side views of System **1** (- 3,7-dihydroxy-1,5-naphthyridine) are based on a 3×2×2 replication of the simulation cell and those for Systems **2** (1,3,5-trioxane-2,4,6-triimine) and **3** (1,3,5-triazine-2,4,6-triol) are based on 2×2×2 replications of the unit cell with the use of periodic boundary conditions. Silver, blue, red, and green spheres indicate carbon, nitrogen, oxygen, and hydrogen atoms, respectively. Thin lines between atoms indicate hydrogen bonds.

The first approach to constructing model systems focused on designing molecular species that could in principle form 2D hydrogen-bonded networks. To do this, HB donors and acceptors are incorporated into or onto single or fused six-membered rings, the resulting molecules are arranged into networks in which HBs exist between the molecules to yield layers, and the structures are relaxed to determine whether the layered structure is stable. The full set of systems considered in this process include System **1**, as well as the systems shown in Figure 3.2. The results of structural optimizations of these systems are discussed briefly in what follows.

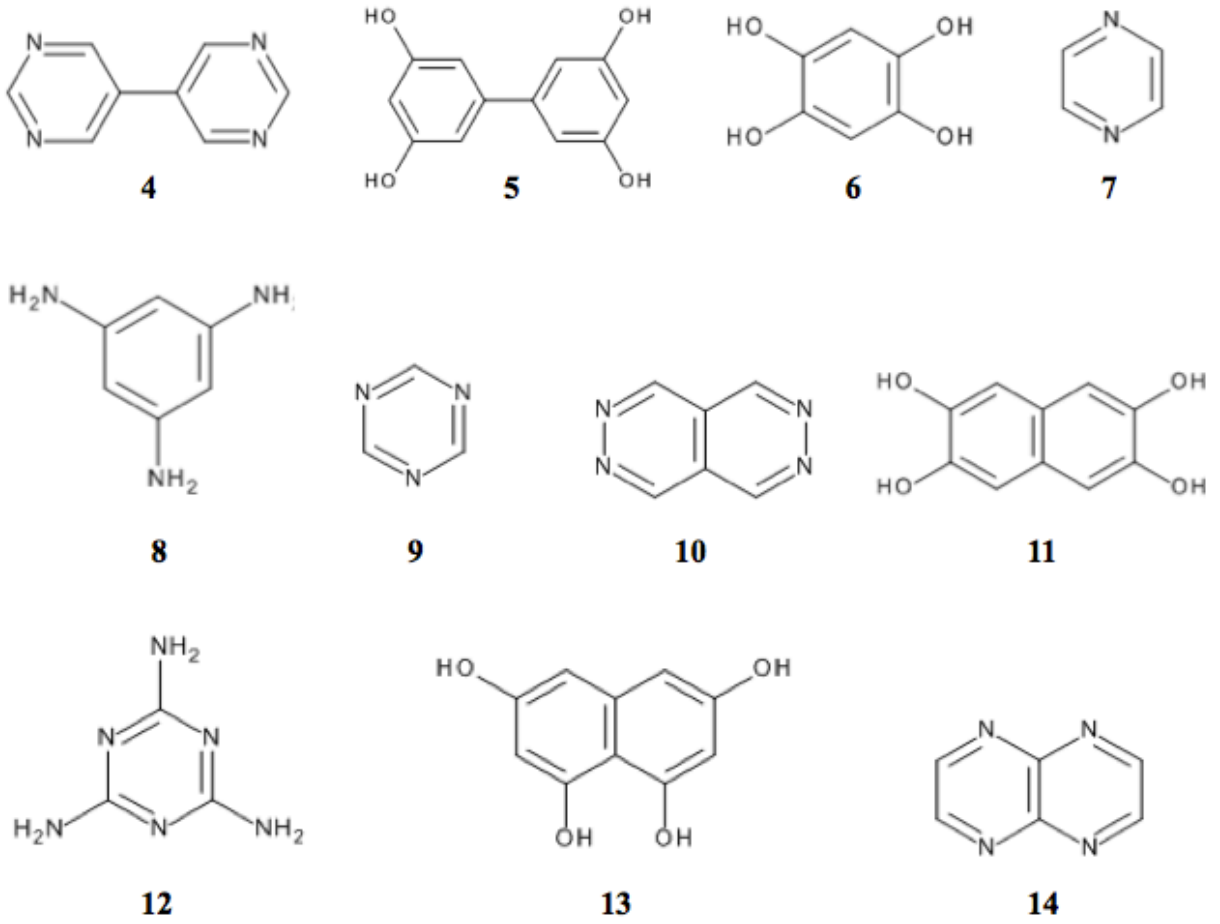

Figure 3.2. Molecular components considered in the formation of two-dimensional hydrogen-bonded networks.

Geometry optimization of a system consisting of a combination of **4** and **5** showed that the ability to adopt a layered configuration is compromised if portions of the molecular components forming the system can rotate out of the plane associated with a layer. In this case, rotation occurred about the central C-C bond of the biaryl groups, which caused the hydrogen bond donors and acceptors to point between layers. These observations indicate that it is important to restrict the abilities of the molecules forming the layers to rotate out of the plane of the layers. As such, additional systems focused on individual rings or fused rings that did not contain rotatable C-C bonds.

A system formed by a mixture of **6** and **7** was developed. Although, this system does not contain rotatable C-C bonds, the alignment of the two nitrogen atoms in **7** was found to provide a rotational axis in the hydrogen-bonded systems. Rotation about this N-N axis occurred and disrupted the layered structures. This indicates that it is important to place the hydrogen bond donors and acceptors at positions that do not introduce rotational axes into the hydrogen bonded layers.

Molecules **8** and **9** contain hydrogen-bond donors and acceptors at alternating positions around six-membered rings. This prevents the introduction of rotational axes between these groups, which would cause the rings to rotate out of the planes associated with each layer. However, the NH_2 group is not planar, which led to hydrogen bonds pointing between molecules in adjacent layers instead of residing within the layers. **12** also contains NH_2 groups. Optimization of a model consisting of molecules **8** and **9** showed that this system did form a lamellar structure. However, the presence of N-H bonds pointing above or below the rings caused the layers in this system to be corrugated instead of flat. These results indicate that it is

also important to restrict the orientations of the hydrogen bond donors and acceptors to inhibit the formation of hydrogen bonds between layers or to ensure the layers remain flat.

Optimization of a system formed by combining **10** and **11** showed that the positions of the hydrogen bond donors and acceptors in these molecules led to long, weak hydrogen bonds and layers with low cohesion energies. Meanwhile, optimization of a structure composed of **13** and **14** led to layers that possessed large empty spaces.

Overall, these results highlight the challenges of forming two-dimensional hydrogen-bonded networks to act as potential lubricants. The results of this model development process showed that layer formation is sensitive to the number and positions of the HB donors and acceptors on the rings, as well as the abilities of the HB donors and acceptors to adopt geometric configurations that cause the HBs between molecular units to reside within the molecular layers without undergoing structural changes that lead to the formation of HBs between layers. Ultimately, this approach to model development led to the identification of the structure labeled System **1** in Figure 3.1 as a system that adopted a 2D layered structure. As shown in that figure, this model system is based on a molecular component consisting of two fused six-membered rings, with each ring containing a nitrogen atom that acts as an HB acceptor and an OH group that acts as an HB donor. Similar fused-membered rings containing nitrogen atoms and bearing hydroxyl groups have been shown to aggregate into 2D structures via HBs.[10] The simulation cell used in the calculations of this system contained two molecular layers stacked on top of one another, with two molecular components per layer. This corresponds to a simulation cell containing 72 atoms.

Whereas the first approach to model design started from molecular components and arranged them into layered structures, the second approach focused on starting with a graphene

sheet and adding molecular components that could be mapped onto the geometry of such a sheet. Specifically, in this approach, model systems were developed by starting with a single layer of graphene, replacing the carbon atoms in the graphene sheet with those in the molecular components forming the self-assembled system, and deleting all remaining carbon atoms in the original graphene sheet at positions that were not included in a molecular component. This process is illustrated schematically in Figure 3.3.

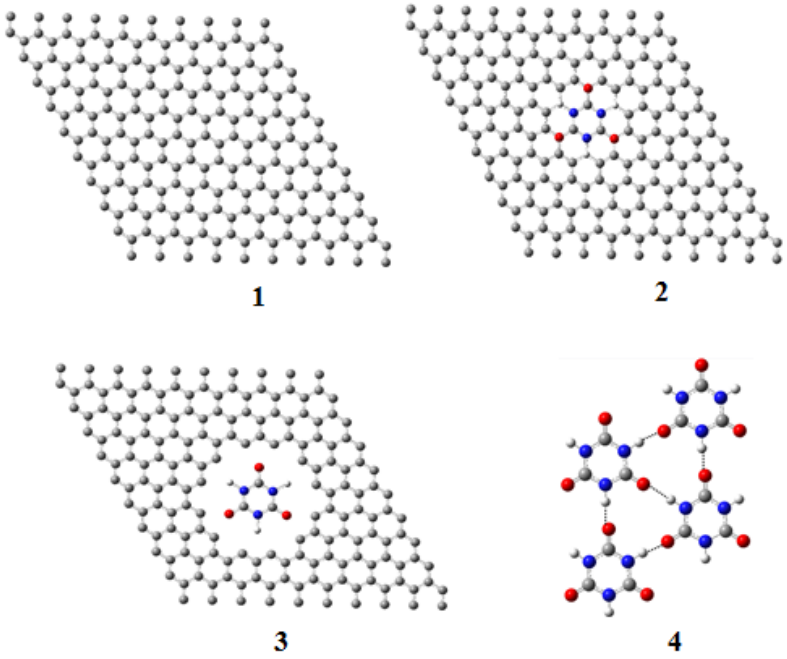

Figure 3.3. Stepwise process outlining the second method used to develop model systems. Step 1 involves starting off with a generated sheet of graphene and in Step 2, carbon atoms are replaced with species designed to act as HB donors and acceptors. In Step 3, all surrounding atoms not involved in the molecular components are deleted. The process is repeated three more times in Step 4 to achieve 4 separate molecules bonded together through hydrogen bonding forming a similar network to that of graphite.

The molecular components employed for this purpose are restricted to six-membered rings containing three HB donors and three HB acceptors at alternating positions on the ring. Three of the atoms in the ring corresponded to sp^2 carbon atoms that were functionalized with either =O or =NH groups. The restriction of the functional groups on the ring to those possessing sp^2

hybridization stemmed from the fact that such groups encourage hydrogen bonding between molecular components within a given layer yet cannot easily rotate to form HBs between layers. The three remaining atoms in the ring were replaced with species possessing sp^3 hybridization, such as NH groups and oxygen atoms. The use of species with sp^3 hybridization at these positions was necessary to ensure the molecules remained neutral when the functional groups with sp^2 hybridization were bonded to the carbon atoms in the ring. Meanwhile, the NH groups or O atoms used at the sp^3 positions can participate in HBs and in electronic conjugation to allow the rings to remain planar. Once constructed, the model systems were relaxed to determine whether they retained the desired layered structure. This approach to model development led to the identification of the two models labeled Systems **2** and **3** in Figure 3.1 as systems that adopt layered geometries. The simulation cells used to study these systems each contained two layers, with four molecular components present in each layer. In both cases, this corresponds to model systems containing 96 atoms. Species containing the functionalities present in the monomers comprising Systems **2** and **3** have been shown to form layered structures. In fact, the monomers in System **3** combine with melamine to form 2D HB networks.[6]

3.2. Computational Details

The structural and dynamic properties of Systems **1**, **2** and **3** (Figure 3.1) were examined through static quantum chemical calculations and FPMD simulations using a version of the Quantum-Espresso software package[11] that was modified to apply predefined strain rates. The use of FPMD simulations permits the examination of any reactions in which these systems may take part, which would not be possible in analogous simulations using standard force fields. The electronic structure was evaluated with Kohn-Sham density functional theory (DFT)[12,13] using the exchange-correlation functional of Perdew, Burke, and Ernzerhof (PBE)[14] plus corrections

for dispersion interactions.[15,16] The PBE functional has been demonstrated previously to provide an accurate description of hydrogen bonding,[17] which is necessary to describe interactions between molecules in the layers comprising the systems in Figure 3.1, whereas the empirical treatment of dispersion has been shown to accurately account for the interactions between species like the molecules comprising these layers.[18] The valence states were represented as a set of planewaves expanded at the Γ-point to a kinetic energy cutoff of 40 Ry and the core states were treated with projector augmented wavefunction potentials.[19] The constant cutoff approach of Bernasconi *et al*. was used throughout.[20]

The dynamics were performed using a time step of 1.0 fs, which conserved total energy to better than 1.0×10^{-5} au/ps in simulations performed in the NVE ensemble. The systems were equilibrated at 300 K using the Andersen thermostat.[21] Temperature controls were removed after equilibration and the systems were sheared along low energy directions identified through potential energy surface scans in which the upper layer was rigidly moved relative to the lower layer. Analysis of the temperatures during these simulations showed that significant heating did not occur prior to the slip events and reactions examined in this study. Shear strains were imposed by orienting the cell such that the layers within each system were aligned with the **a** and **b** lattice vectors, which also spanned the *x*-*y* plane, and then altering the *x* and *y* components of the **c** lattice vector such that the top of the simulation cell moved a distance, Δx, along the slip direction at a rate of 1.0 Å/ps using Lees-Edwards boundary conditions.[22] Additional simulations of System **3** performed at lower sliding rates of 0.2 and 0.5 Å/ps indicated that the slip mechanism is not dependent on the sliding velocity. The *z* component of **c** was allowed to vary to maintain predefined normal stresses ranging from 0 to 10 GPa using the method of Parrinello

and Rahman.[23] The lateral components of the simulation cell spanned the *x*-*y* plane and were fixed during shearing.

3.3. Structural and Energetic Details of the Model Systems

Key structural and energetic features of the systems in Figure 3.1 were determined through static quantum chemical calculations. The calculated quantities are summarized in Table 3.1 and discussed in this section.

Table 3.1. Interlayer thicknesses, d (Å), in-layer areal atomic densities, ρ_A (atoms/Å^2), energy of each system relative to the separated monomers, E_{rel} (kJ/mol·monomer), surface energies, E_{surf} (J/m^2), interaction energies between monomers, E_{int} (kJ/mol·monomer), and HB energies, E_{HB} (kJ/mol) for Systems **1**, **2**, and **3**.

System	d	ρ_A	E_{rel}	E_{surf}	E_{int}	E_{HB}
1	2.796	0.367	-282.3	0.217	-154.3	77.2
2	2.854	0.252	-122.2	0.098	-65.9	22.0
3	2.847	0.306	-165.2	0.147	-96.9	32.3

The side views of the structures in Figure 3.1 illustrate that all three systems can form well-ordered layered structures. The interlayer separation, d in Table 3.1, is similar for all systems, with this distance ranging from 2.796 to 2.854 Å. Notable differences regarding the structures of the layers exist for these three systems. System **1** is clearly distinct from Systems **2** and **3** because the monomers in it each contain two fused six-membered rings, whereas the monomers in Systems **2** and **3** each contain one six-membered ring. In all systems, the monomers are connected via HBs. In **1**, the HBs involve hydroxyl groups acting as HB donors and nitrogen atoms in the rings acting as HB acceptors, with each monomer involved in two HB donating and two HB accepting interactions. This arrangement of HBs allows each monomer in system **1** to interact with four other monomers via HBs, which leads to an approximately hexagonal

arrangement of monomers within each layer. The monomers of System **2** are connected via HBs between NH groups bonded to the six-membered rings. Meanwhile, the atoms within the six-membered rings are not involved in any significant interactions between monomers in the same layer. The positions of the NH groups on the monomers, symmetric nature of the monomers, and lack of participation of atoms in the six-membered rings in HB interactions cause the monomers comprising System **2** to adopt a hexagonal arrangement with the rings separated by large spaces that contain no atoms. The monomers comprising System **3** are connected via HBs between NH groups within the six-membered rings and carbonyl groups extending from those rings. The participation of groups within the rings in HB interactions, as well as the symmetric nature of those interactions around each monomer, results in the monomers in System **3** adopting a hexagonal arrangement with a low amount of empty space around each monomer when compared to System **2**. The energies of each system relative to the separate monomers, E_{rel}, in Table 1 indicate that each of these systems are stable with respect to the separated monomers, with the stabilities of the systems increasing as **2** < **3** < **1**.

The interlayer interaction strength can play a key role in tribological performance, with strong adhesive interactions leading to larger friction forces.[24–27] The strengths of the interactions between the layers were obtained by evaluating the surface energy, E_{surf}:

$$E_{surf} = \frac{E_{layer} - 0.5E_{bulk}}{2A} \qquad \text{(Eq. 3.1)}$$

where E_{bulk} is the energy of a single simulation cell containing two layers, E_{layer} is the energy of a single layer, and A is the cross-sectional area. The data in Table 3.1 show that the values of E_{surf} are ordered as **2** < **3** < **1**. This trend can be rationalized by recognizing that the interactions

between the layers are dominated by attractive dispersion interactions between the atoms in adjacent layers. In fact, decomposing the surface energies into contributions from dispersion interactions and the remaining contributions to the energy from DFT, shows that the bulk systems are unstable with respect to the separated layers in the absence of dispersion interactions. In accordance with the values of E_{surf}, the contributions of dispersion interactions between layers to stabilizing the bulk systems increase in the order **2** < **3** < **1**. These trends can be explained in terms of the structural details of the systems. Specifically, the areal atomic densities, ρ_A, within the layers increase as **2** < **3** < **1**, which suggests the number, and hence total strength, of the dispersion interactions between layers should increase in the same order. In the context of low-friction materials, the surface energies in Table 3.1 can be compared with those of other two-dimensional materials employed in tribological applications such as graphite (0.106 to 0.122 J/m^2)[28] and MoS_2 (0.047 J/m^2).[29]

The strengths of the interactions between monomers within a layer contributes to the ability of the system to resist structural changes such as dissociation and reorganization. The interaction strengths, E_{int}, between monomers in a layer were evaluated as:

$$E_{\text{int}} = \frac{E_{layer} - NE_{mon}}{N} \qquad \text{(Eq. 3.2)}$$

where N is the number of monomers in a layer and E_{mon} is the energy of a monomer. The data in Table 3.1 show that the values of E_{int} are ordered as **2** < **3** < **1**. These data suggest that the layers in System **1** may be more resistant to decomposition via the dissociation of HBs than those in Systems **2** and **3**. This is somewhat surprising because E_{int} is dominated by HB interactions, with smaller contributions from dispersion interactions between monomers, and the monomers in

System **1** are each involved in fewer HB interactions than those in Systems **2** and **3**. The values of E_{int} were divided by the number of HBs in which each monomer is involved to estimate the average HB strengths for each system. These calculations yielded HB energies, E_{HB}, of 77.2, 22.0, and 32.3 kJ/mol for Systems **1**, **2**, and **3**, respectively. This calculation assumes that E_{int} is derived entirely from HBs, whereas other interactions between the monomers also contribute to E_{int}. As such, this calculation likely overestimates the values of E_{HB}. The values of E_{HB} for Systems **2** and **3** are consistent with weak to moderate strength HBs and the lengths of the HBs in systems **2** and **3** (1.98 and 1.72 Å, respectively) are also consistent with weak to moderate HB interactions. Meanwhile, the HB energy and distance (1.56 Å) for System **1** is consistent with a strong HB.[30]

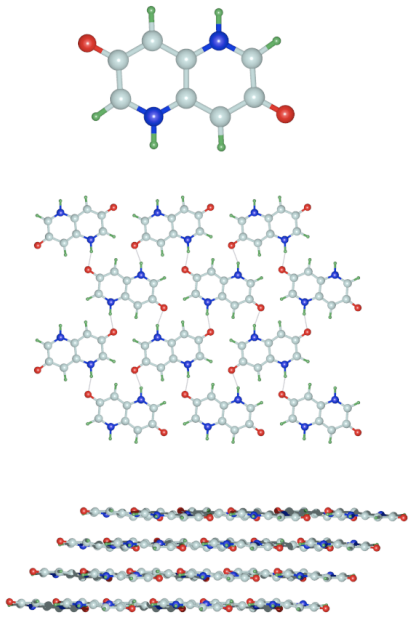

Figure 3.4. Structure of System **1b**. The upper panel shows the molecular species on the network is based, the middle panel shows a top view of a single layer of the system, and the bottom panel shows a side view of the system to illustrate the layered structure. To aid in visualizing the extended structure, a 3×2×2 replication of the simulation cell is shown. Silver, blue, red, and green spheres indicate carbon, nitrogen, oxygen, and hydrogen atoms, respectively. Thin lines between atoms indicate hydrogen bonds.

FPMD simulations of System **1** (*vide infra*) showed that the transfer of protons from a hydroxyl group in one monomer to a nitrogen atom in an adjacent monomer is facile. The proton transfer reaction causes the monomers in **1** to adopt the isomeric structure labeled **1b** in Figure 3.4. Gas-phase calculations of the monomers of **1** and **1b** indicate the former is 84.1 kJ/mol more stable than the latter. This is not surprising because the oxygen and nitrogen atoms of **1b** bear formal charges of -1 and +1, respectively, and the formation of zwitterions is generally unfavorable in a vacuum. Meanwhile, the calculations show that **1** is more stable than **1b** by 0.22 kJ/mol·monomer in the condensed phase when the structure is optimized in a cell defined by the optimal lattice vectors for **1**. Relaxing the atomic positions and lattice vectors of **1b** causes the structure to be more stable than **1** by 14.92 kJ/mol·monomer. This suggests that the proton affinities of the nitrogen atoms in **1** are high in the condensed phase, which may lead to stronger interactions between monomers than one would anticipate on the basis of HB interactions alone.

3.4. Shearing Systems 1, 2, and 3 in the Absence of a Normal Load

The structural optimizations showed that Systems **1**, **2**, and **3** have different structural features, as well as different interlayer and intralayer interaction strengths. FPMD simulations were performed in which these systems were sheared in the absence of a normal load to gain insight into structural changes that may occur within these systems when exposed to shear stresses and to evaluate their abilities as lubricants. The directions in which shear strain was imposed were chosen to correspond to the lowest energy pathway on a potential energy surface obtained by moving the upper layer relative to the bottom layer over a set of fixed increments.

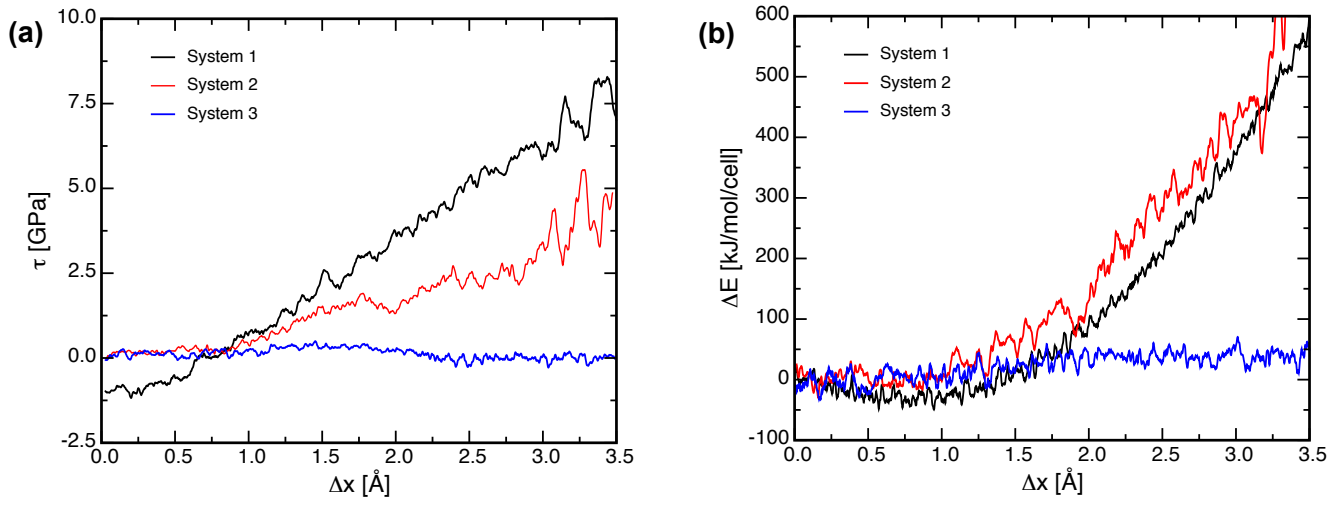

Figure 3.5 (a) Shear stress, τ, versus shear distance, Δx, for Systems **1**, **2**, and **3**. The data illustrate significant differences between all three systems, with System **1** exhibiting a strong resistance to shear over the entire range of Δx, System **2** shearing easily at low Δx before exhibiting a steady increase in τ, and System **3** exhibiting low τ for all Δx. (b) Potential energy, ΔE, versus Δx for Systems **1**, **2**, and **3**. The data show that system **1** passes through a potential energy minimum at Δx = 0.8 Å, System **2** exhibits an energy profile that increases rapidly for Δx > 0.8 Å, and System **3** exhibits a flat energy profile with a slight increase in ΔE when Δx = 1.5 Å. In all cases, the energies have been shifted such that ΔE = 0.0 kJ/mol/cell when Δx = 0.0 Å.

The shear stresses, τ, and potential energies, ΔE, for Systems **1**, **2**, and **3** are plotted in Figures 3.5a and 3.5b, respectively, versus the shear distance, Δx, which is defined as the distance the upper point of the simulation cell has moved along the shear direction. The data show that all three systems respond to shear in markedly different ways. For System **1**, τ increases linearly from a value of approximately -1.0 GPa at Δx = 0.0 Å at a rate of approximately 2.7 GPa/Å without exhibiting a sharp peak followed by a sharp drop in τ that would be consistent with a slip event. For System **2**, τ is flat from Δx = 0.0 to 0.8 Å and then increases to reach a local maximum of $\tau \approx$ 1.5 GPa at $\Delta x \approx$ 1.75 Å that is associated with a slip process. However, τ does not return to zero at this point, but rather drops slightly to ~1.25 GPa

followed by a steady increase with further increases in Δx. The τ-Δx relationship is nearly flat for System **3**, with a maximum value of $\tau \approx 0.6$ GPa being reached when the system slips at $\Delta x = 1.5$ Å. The origins of the different responses of these systems to being sheared are examined below.

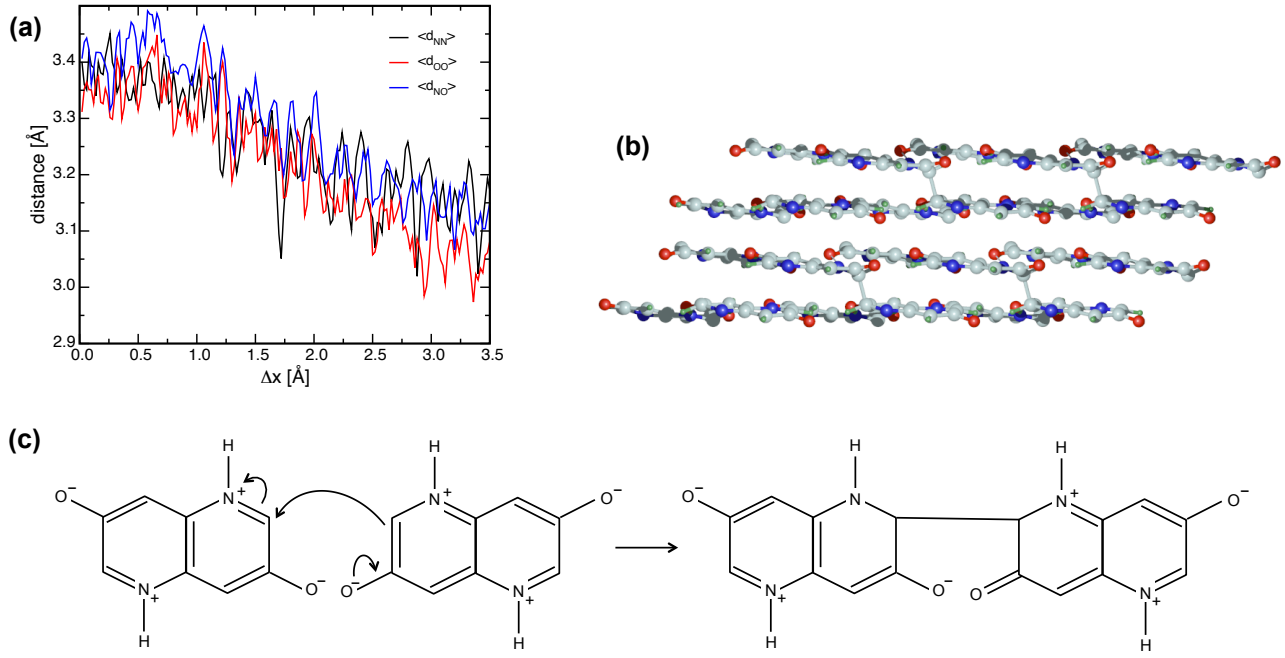

Figure 3.6. (a) Average values of the shortest N-N, O-O, and N-O distances involving N and O atoms in adjacent layers of System **1** versus Δx. The data show that these distances decrease steadily with increasing Δx. (b) Structure of system after the formation of C-C bonds between layers at $\Delta x = 3.0$ Å. Silver, blue, red, and green spheres represent carbon, nitrogen, oxygen, and hydrogen atoms, respectively. (c) Proposed mechanism for the C-C bond formation process.

System **1** exhibits the largest resistance to shear of the three systems considered. This behavior can be understood by considering how structural changes that occurred within the system affect the abilities of the layers comprising the system to move past one another. The FPMD simulations showed that extensive proton transfer occurred between the monomers in System **1** even prior to shear, resulting in layers composed of isomer **1b**. This change in structure

is responsible for the negative values of τ below Δx = 0.8 Å because the simulation was initiated with the x and y components of the **c** lattice vector set to the optimal values for System **1**, whereas the optimal values for System **1b** are reached closer to Δx = 0.8 Å. This is evident from the data in Figure 3.5b, which show that System **1** passes through a potential energy minimum along the shear direction when Δx = 0.8 Å. After this point, ΔE increases with Δx in an approximately quadratic manner, which is consistent with the linear τ-Δx relationship.

As noted above, the proton transfer process causes the oxygen and nitrogen atoms in this system to bear formal charges of -1 and +1, respectively. While these represent formal charge values, in practice these atoms will bear partial charges. Löwdin population analysis[31,32] of the electronic structure of **1b** at its optimized configuration in the condensed phase showed that the oxygen atoms bear charges of -0.50 and the nitrogen atoms bear charges of -0.15, with small positive fractional charges on the other atoms in the system. The presence of charged atoms within the layers will cause the interlayer strength to be dominated by Coulomb interactions, which are sensitive to the distances between the charged atoms. To investigate how these distances change during the slip process, the minimum distance between each nitrogen or oxygen atom in one layer and another nitrogen or oxygen atom in an adjacent layer were calculated for all nitrogen and oxygens in the system. These values were sorted according to N-N, O-O, and N-O interactions and averaged for each type of interaction. The resulting averaged minimum separations are shown versus Δx in Figure 3.6a. The data show that the distances associated with all three types of interactions between charged atoms change very little or even increase slightly between Δx = 0.0 and 0.8 Å, which corresponds to the range of Δx over which τ is negative for this system. Meanwhile, the relative movement of the layers as the system is sheared causes the minimum separation between charged atoms to decrease in an approximately linear manner at

higher values of Δx. This behavior causes the system to move from a region with low interlayer electrostatic repulsion to one with higher interlayer electrostatic repulsion during the slip process. In a relative sense, this results in the system moving from a lower energy region to a higher energy region, which in turn resists shear. This is true if one considers the oxygen and nitrogen atoms as bearing formal charges of -1 and +1, respectively, or if one considers these atoms as possessing fractional charges with negative values. In the former case, the N-N and O-O interactions will be repulsive, while the N-O interactions will be attractive. However, the total number of N-N and O-O interactions will be greater than the number of N-O interactions, and hence the net effect of these interactions will be repulsive. In the case where the oxygen and nitrogen atoms bear negative fractional charges, all these interactions will be repulsive. In either case, the interactions between the layers will resist shear. Similar effects of the presence of ions upon the shear stresses of layered silicates have been noted previously.[33]

The data in Figure 3.5 also indicate that System **1** does not undergo a clear slip process, which would be characterized by a local maximum in τ when slip occurred followed by a rapid drop to τ = 0.0 GPa as the system moves to the next local energy minimum along the slip direction. Instead, τ increases steadily over the entire range of Δx considered. The absence of a slip event is due to the formation of a C-C bond between layers at $\Delta x \approx 3.0$ Å. The product of this reaction is shown in Figure 3.6b and the associated reaction mechanism is outlined in Figure 3.6c. Essentially, this reaction neutralizes some of the formal charges on the atoms in the system and occurrs readily when the relevant carbon atoms, i.e. those residing between the nitrogen atoms and carbonyl groups in the rings, were brought into sufficiently close proximity to react as the system is sheared. This process can occur repeatedly at different sites in the system as the imposition of shear strains brings these reactive carbon atoms close together, which will

ultimately result in a system with covalent bonds between the layers. Such systems will not be effective in the context of lubrication, and hence the behavior of System **1** when sheared was not examined further in the context of lubrication.

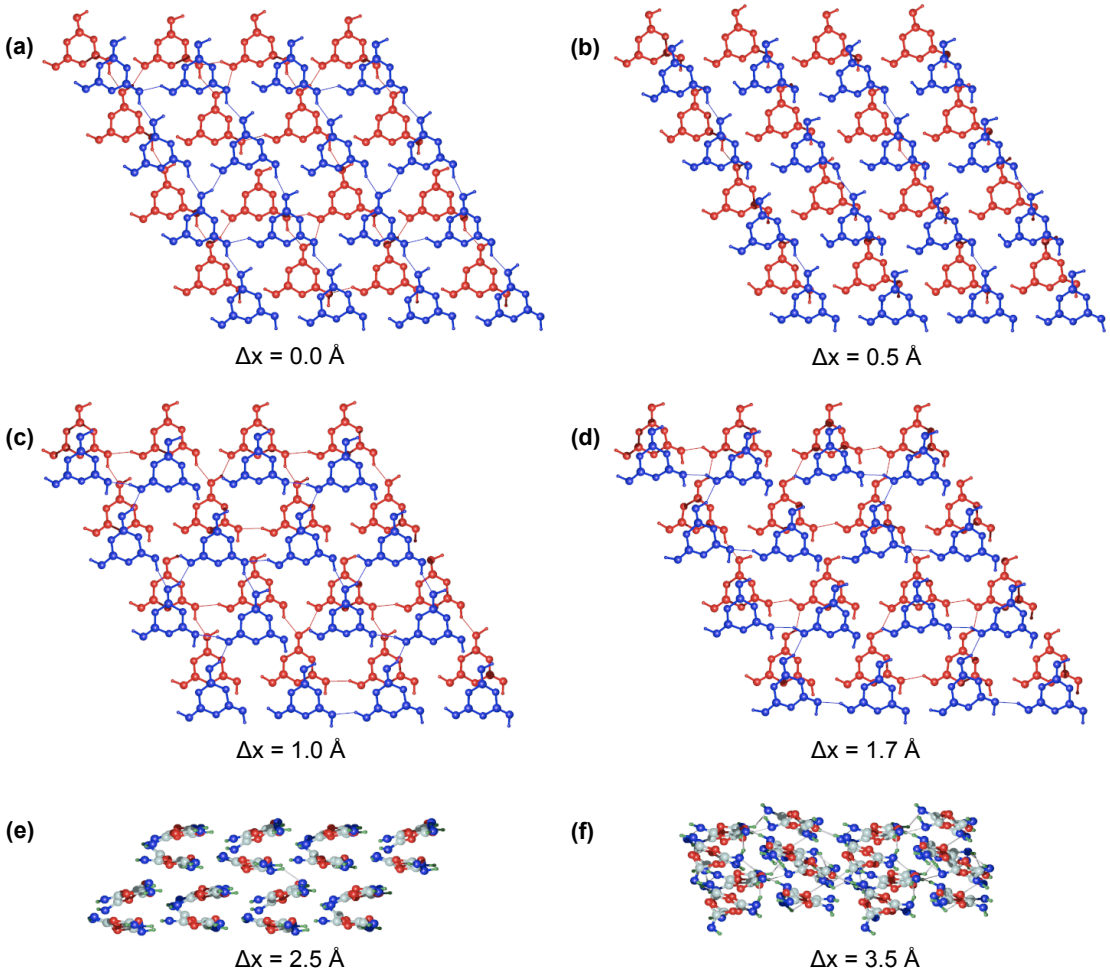

Figure 3.7. (a) through (d) correspond to top-down views of System **2** at Δx = 0.0, 0.5, 1.0 and 1.7 Å. (e) and (f) correspond to side views of system 2 at Δx = 2.5 and 3.5 Å. The top-down views illustrate the relative motion of adjacent layers during shear. This process increases the overlap between rings in adjacent layers in a manner that accounts for the τ-Δx relationship for Δx below 1.7 Å in Figure 3.5. The side views illustrate the reorganization of System **2** due to the formation of HBs between layers. In the top-down views, all atoms in the upper and lower layers have been colored blue and red, respectively. In the side views, silver, blue, red, and green spheres represent carbon, nitrogen, oxygen, and hydrogen atoms, respectively.

The values of τ for System **2** are close to 0.0 GPa until Δx reaches approximately 0.8 Å, after which τ increases with Δx at a rate of 1.7 GPa/Å. This behaviour can be understood by examining the structures of the system when shear. Top-down views of two adjacent layers of this system at points between Δx = 0.0 Å and Δx = 1.7 Å are shown in Figure 3.7. The structures show that when Δx = 0.0 Å, the layers are arranged such that the rings in the bottom layer are largely aligned with holes in the top layer and the rings in the top layer occupy positions over HBs in the bottom layer. The application of shear strain to reach Δx = 0.5 Å causes the structure to change very little, with the rings in the upper layer undergoing slight changes in orientation and the loss of some HBs within the layers. The similarities between the structures at Δx = 0.0 Å and Δx = 0.5 Å suggest that moving between these two structures is a low energy process, with the calculated energies indicating that these systems differ in potential energy by 10 ± 20 kJ/mol·cell. This small change in energy is consistent with the flat τ-Δx relationship for Δx below 0.8 Å. The structure at Δx = 1.0 Å differs markedly from those at Δx = 0.0 and 0.5 Å. Specifically, the layers have moved relative to one another in a manner that increases the overlap between the molecular components in adjacent layers. The increase in this overlap will increase the interlayer interaction energy, which causes the system to resist shear in a manner consistent with the steady increase in τ between Δx = 0.8 and 1.7 Å. Slip occurs at Δx ~1.7 Å where a local maximum is present in the τ-Δx curve. The structure at this point shows even further overlap between the molecular components, with the relative energies of the structures at Δx = 0.0 and 1.7 Å yielding a slip barrier of 107 ± 20 kJ/mol/cell. Overall, the changes in the relative positions of the layers during shear accounts for the shape of the τ-Δx plot prior to slip.

As noted above, τ does not return to 0.0 GPa for System **2** after slip occurs at Δx ~ 1.7 Å, but rather drops to a value of ~1.2 GPa before increasing again with further increases in Δ*x*. The potential energy in Figure 3.5b show that the system briefly drops into a local energy minimum at this point, followed by a rapid increase in energy. The origin of this behavior is evident from an examination of the structures the system adopted at higher values of Δ*x*. Side views of the structures with Δ*x* = 2.5 Å and 3.5 Å are shown in Figure 3.7. These structures can be compared with the optimized structure of System **2** shown in Figure 3.1. Clearly, in the optimized structure of the system, the monomers are arranged into well-defined layers. This layered structure persisted up to the point at which slip occurred at Δ*x* = 1.7 Å. By comparison, the structure at Δ*x* = 2.5 Å shows that the monomers have rotated within each layer and are potentially interacting with monomers in neighboring layers. Such interactions are problematic from the standpoint of maintaining an easily shearable layered system that can be used for the purposes of lubrication. While the structure at Δ*x* = 2.5 Å resembles a layered structure, albeit with rotated monomers within each layer, the structure at Δ*x* = 3.5 Å does not. The impact of this structural reorganization is evident from the *τ*-Δ*x* plot in Figure 3.5, with *τ* approaching 5 GPa as the system adopts the structure at Δ*x* = 3.5 Å.

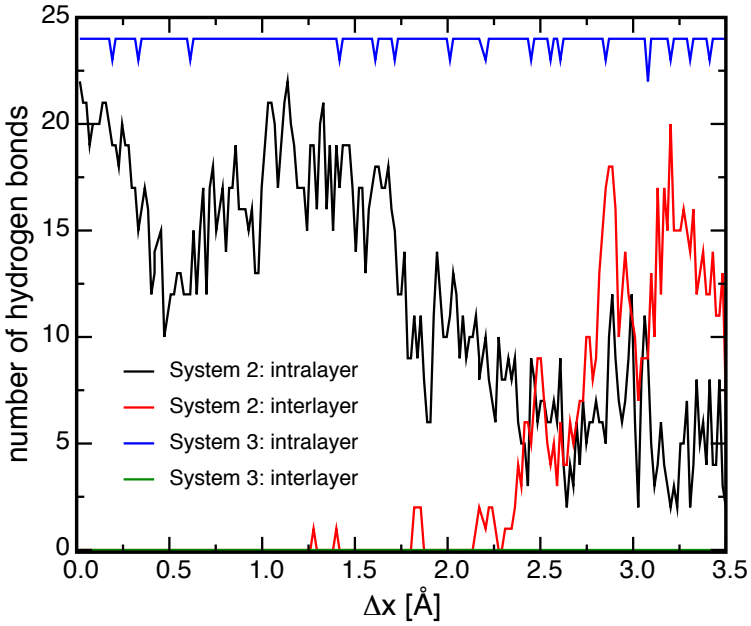

Figure 3.8. Number of inter- and intralayer HBs for Systems **2** and **3** versus Δx. The maximum possible number of intralayer HBs is 24 for both systems. The data show that intralayer HB dissociation occurs readily for System **2**, and interlayer HB formation occurs at higher values of Δx. The data also show that the intralayer HBs are stable for System **3** and that no interlayer HB formation occurs for this system.

The loss of well-defined layers in System **2** is due to changes in the direction of HBs in the system. To illustrate this, the total number of HBs within the layers and between the layers in the system were calculated over Δx with the molecules in a given layer defined according to the structure present at Δx = 0.0 Å. These values are plotted in Figure 3.8. In the construction of this figure, an HB was determined to exist if the distance between the H atom in an HB donor and the atom (N or O) in the HB acceptor was between 1.5 and 2.25 Å without any consideration of angles. While more sophisticated means of identifying HBs exist, this simple distance-based approach is adequate for the purpose of illustrating how the HBs within and between the layers in these systems change during shear. The data in this figure show that the number of intralayer HBs in System **2** is reduced significantly from the maximum possible value of 24, which is present in the optimized structure. This is a consequence of the relatively weak nature of the HBs

in this system (see Table 3.1 for HB strengths). The dissociation of the HBs results in free HB donors and acceptors that can interact with HB donors and acceptors in other layers to lead to structures like those shown in the bottom panels of Figure 3.7. The data in Figure 3.8 show that no, or very few, interlayer HBs are formed for Δx below 2.5 Å. This is consistent with the system retaining a structure with well-defined layers. Meanwhile, the number of interlayer HBs increases rapidly for Δx above 2.5 Å, with the number of interlayer HBs exceeding the number of intralayer HBs at Δx ~2.8 Å. This change in the directions of the HBs is a consequence of the relative movements of the layers in the system and the relative weak nature of the HBs in the system. At low Δx the groups that can form HBs in adjacent layers are too far apart to form HBs. Meanwhile, as the system is sheared, the molecular components in one layer become more closely aligned with those in adjacent layers, which provides a means for HB formation between layers to occur. The formation of these interlayer HBs may be responsible for the increased shear stresses observed for System **2** at higher values of Δx, since previous work has illustrated that interlayer HBs lead to increased shear strengths.[7,8]

System **3** exhibits a nearly flat τ-Δx plot with a maximum of τ = 0.6 GPa at Δx ~ 1.5 Å that can be associated with the initiation of a slip process. Key structures associated with the slip process are shown in Figure 3.9. When Δx = 0.0 Å, the molecules in the upper and lower layers are offset from one another, such that the molecules in one layer reside primarily over holes in the adjacent layer. The structure at Δx = 1.5 Å, shows that shearing the system causes the rings in a given layer to move over HBs in the adjacent layers instead of moving in a way that leads to a significant overlap between the atoms in the adjacent layers. As a result, the interlayer interaction strength remains low, with the relative energies of the structures at Δx = 0.0 and 1.5 Å yielding an estimated slip barrier of 50 ± 19 kJ/mol/cell, which results in low shear stresses being

required to induce slip in this system. The product of the slip event was examined by continuing to shear the system until Δx = 5.0 Å was reached. Although the associated values of τ are not shown in Figure 3.5, they continued to remain close to 0.0 GPa. The slip product, which corresponds to the structure at Δx = 5.0 Å in Figure 3.9, is analogous to that at Δx = 0.0 Å, with rings in one layer residing over holes in the adjacent layer. Continued movement of the layers along the shear direction from this point would result in rings passing over one another. However, the FPMD simulations indicate that the layers move relative to one another in the lateral dimensions to follow a slip path originating from the structure at Δx = 5.0 Å that is rotated by 60° with respect to the initial slip direction. This path is symmetrically equivalent to the original slip direction and will thus incur low shear stresses for slip to occur.

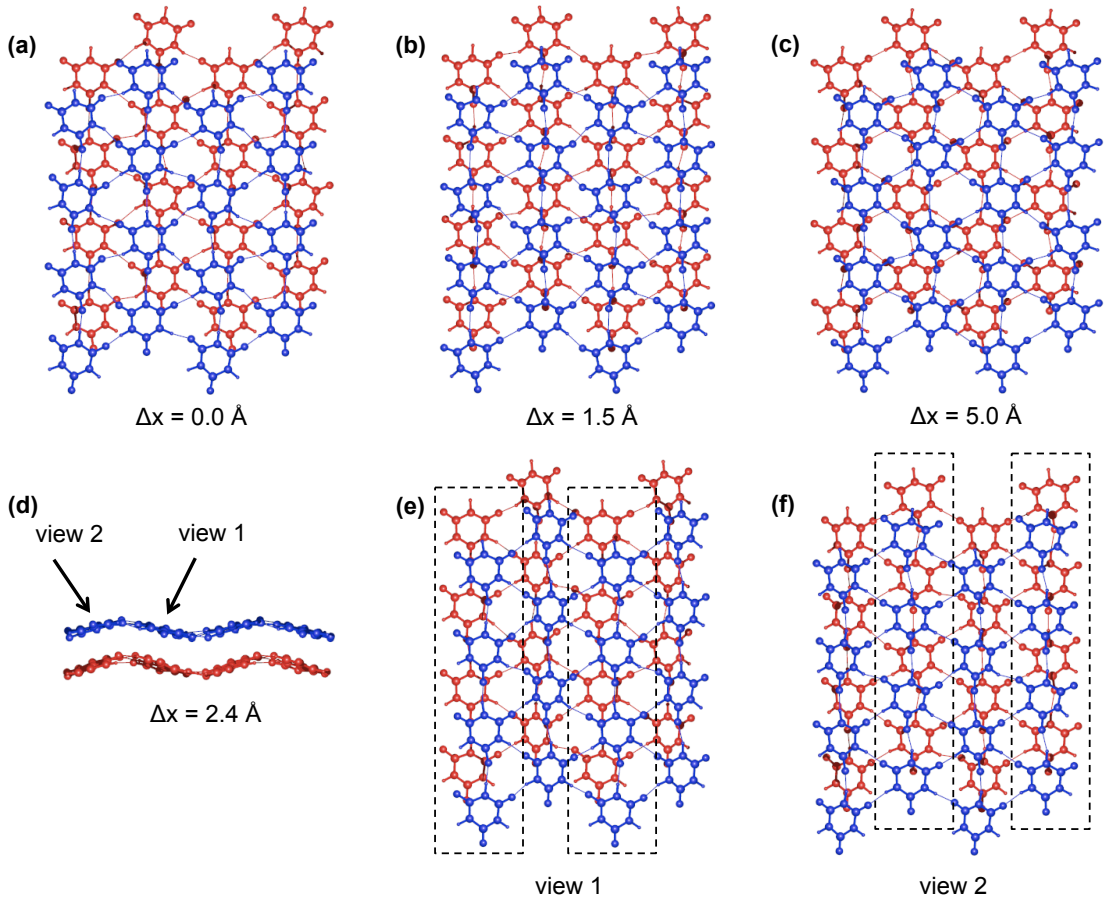

Figure 3.9. (a) through (c) correspond to top-down views of System **3** at Δx = 0.0, 1.5 and 5.0 Å. The structure at Δx = 0.0 Å shows how the layers are arranged such that rings in one layer are aligned with holes in adjacent layers. The structure at Δx = 1.5 Å corresponds to that at which slip occurs, with the rings in one layer moving over HBs in adjacent layers. The structure at Δx = 5.0 Å corresponds to the product of slip and has a structure similar to that at Δx = 0.0 Å. (d) through (f) correspond to the structure at Δx = 2.4 Å observed along various directions. The side view in (d) illustrates the buckling that occurs within the layers during the slip process. The view in (e) shows how the buckling has allowed one pair of molecular strands in the system (indicated by the dashed box) to move past one another. The view in (f) shows how the second pair of molecular strands (indicated by the dashed box) have not slipped past one another. All atoms in the upper and lower layers have been colored blue and red, respectively.

Analysis of the structures between Δx = 1.5 and 5.0 Å showed that slip occurred through a process that allowed aligned strands of overlapping rings, which consist of sets of rings aligned vertically in the page in the top-down views of the structures in Figures 3.9a-c, to move past one another in a stepwise manner. This process involves the deformation of the layered structures

such that each layer becomes buckled as illustrated by the side view of the structure at Δx = 2.4 Å in Figure 3.9. This buckled arrangement allows the strands of rings to move past one another in a successive manner. This type of motion is evident from the structures at Δx = 2.4 Å along Views 1 and 2, which correspond to directions perpendicular to the rings in adjacent strands. The structure along View 1 illustrates that the rings in one set of strands (contained in dashed boxes) have moved past one another and adopted a configuration similar to that in the product. Meanwhile, the structure along View 2 illustrates that the rings in the other set of adjacent strands (contained in dashed boxes) overlap in a manner similar to the rings in the structure at Δx = 1.5 Å. After the second strand of rings moves past one another at Δx = 4.4 Å, the layers revert to a flat structure. By reducing the number of molecular components that move past one another at a given value of Δx, the stepwise slip process can lead to a lower slip barrier, and hence lower shear strength, than an alternative process in which the layers remain flat and move rigidly past one another. This point is discussed in greater detail in Section 3.5, where the slip mechanism of System **3** is examined over a range of applied normal loads.

Overall, these results indicate that System **3** may be an effective lubricant, with the system exhibiting a low shear strength along with the ability to undergo significant deformations while retaining a layered structure. The ability of System **3** to exhibit such behavior is a result of the strong HB network, which is sufficiently strong to persist throughout the entire slip process, but sufficiently weak to permit buckling without incurring a large energetic penalty. The persistence of the HB network is evident from Figure 3.8, which shows that the system remains near the maximum possible number of 24 HBs throughout the entire slip process, with brief decreases from this value arising from fluctuations in the HB lengths near the distance cutoff used to identify HBs. In addition, no interlayer HBs were identified at any point during the simulation.

By contrast, the deformation of covalently-bonded layered systems likely incurs a high energetic penalty, and thus will not be an effective means of lowering shear strengths in such systems. This illustrates a potential advantage of hydrogen-bonded networks over covalently-bonded systems in the context of lubrication.

3.5. Shearing System 3 at Higher Normal Loads

The results reported in the previous section showed that System **3** had a low shear strength of τ_c = 0.6 GPa and underwent a slip process that allowed the system to retain a layered structure that will facilitate subsequent slip events at low shear stresses. As such, this system has the potential to be an effective lubricant. Meanwhile, Systems **1** and **2** exhibited behavior that is undesirable from the standpoint of lubrication, with the former undergoing reactions between atoms in adjacent rings and the latter undergoing structural reorganization to lose its layered structure. In both cases, these behaviors lead to large shear stresses, suggesting that such systems would not be effective as lubricants.

Lubricants are often exposed to a wide range of loads during operation. To explore the behavior of System **3** under these conditions, a series of simulations were performed in which this system was sheared along the same direction as that considered above while simultaneously being exposed to loads, L, applied normal to the slip plane. L = 0.0, 3.9, 7.8, 11.7, and 15.6 nN were considered, which correspond to normal pressures, P, of 0, 2.5, 5, 7.5, and 10 GPa. Three independent simulations were performed at each L. The results of these simulations provide access to the friction coefficient, which quantifies the relationship between friction forces, F_f, and L, as well as an examination of the effect of L on the slip mechanism.

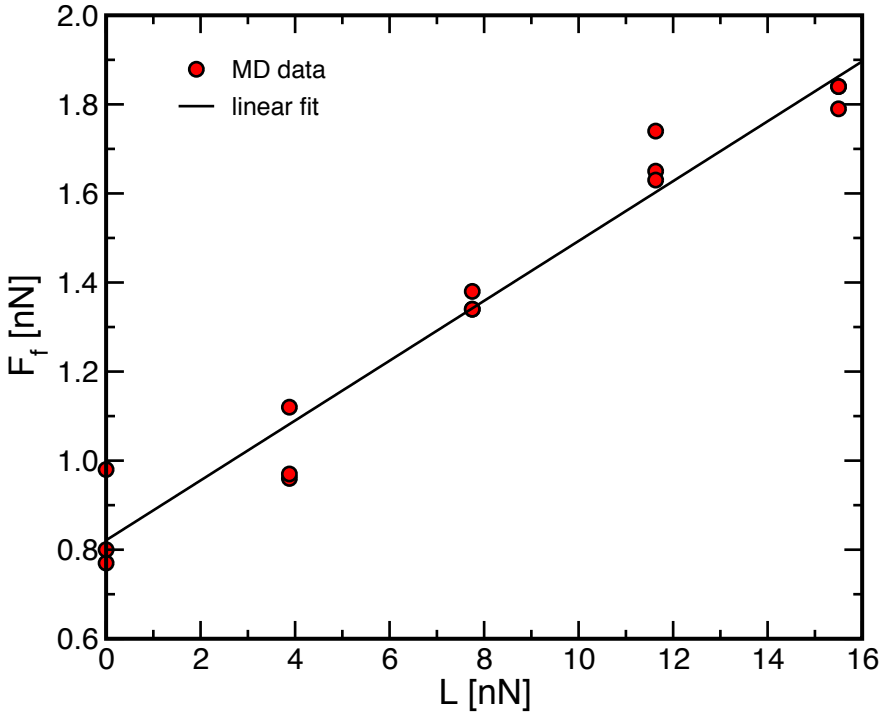

Figure 3.10. Friction forces, F_f, versus normal load, L, for System **3**. Three independent simulations were performed at each L. The symbols correspond to the values of F_f obtained through those simulations. The solid line is a line of best fit through all the data and yields a friction coefficient of $\mu = 0.067 \pm 0.004$.

The calculated values of F_f are plotted against L in Figure 3.10 for the simulations of System **3** performed at different L. The values of F_f were obtained by multiplying the value of τ at the point at which slip occurred by the cross-sectional area, A, of the system. The data in Figure 3.10 show that some spread exists between the values of F_f obtained from independent simulations performed at each L, with the spread being more prominent at low L. While the spread in F_f is large in a relative sense in some cases, this is simply due to the fact that the values of F_f are low and there is a relatively large amount of noise in the τ-Δx plots like those in Figure 3.5a, which were used to obtain F_f. Despite the spread in the values of F_f at each L, there is a linear relationship between F_f and L, which is expected from standard models of friction.[24–27] A line of

best fit through all data points is also provided in Figure 3.10. The slope of the line corresponds to the friction coefficient, μ, whereas the intercept represents an intrinsic friction force that must be overcome due to interactions between layers in the system. The estimated friction coefficient is $\mu = 0.067 \pm 0.004$, whereas the estimated intrinsic friction force is $F_0 = 0.82 \pm 0.04$ nN. The value of μ is low, and can be compared with those of other systems such as graphite ($\mu \approx 0.1$),[34] MoS_2 ($\mu \approx 0.004 - 0.2$),[35,36] and BN ($\mu \approx 0.23 - 0.25$)[37] under various conditions. Overall, these results indicate that System **3** has a low intrinsic friction force and low friction coefficient, and may thus be a useful lubricant.

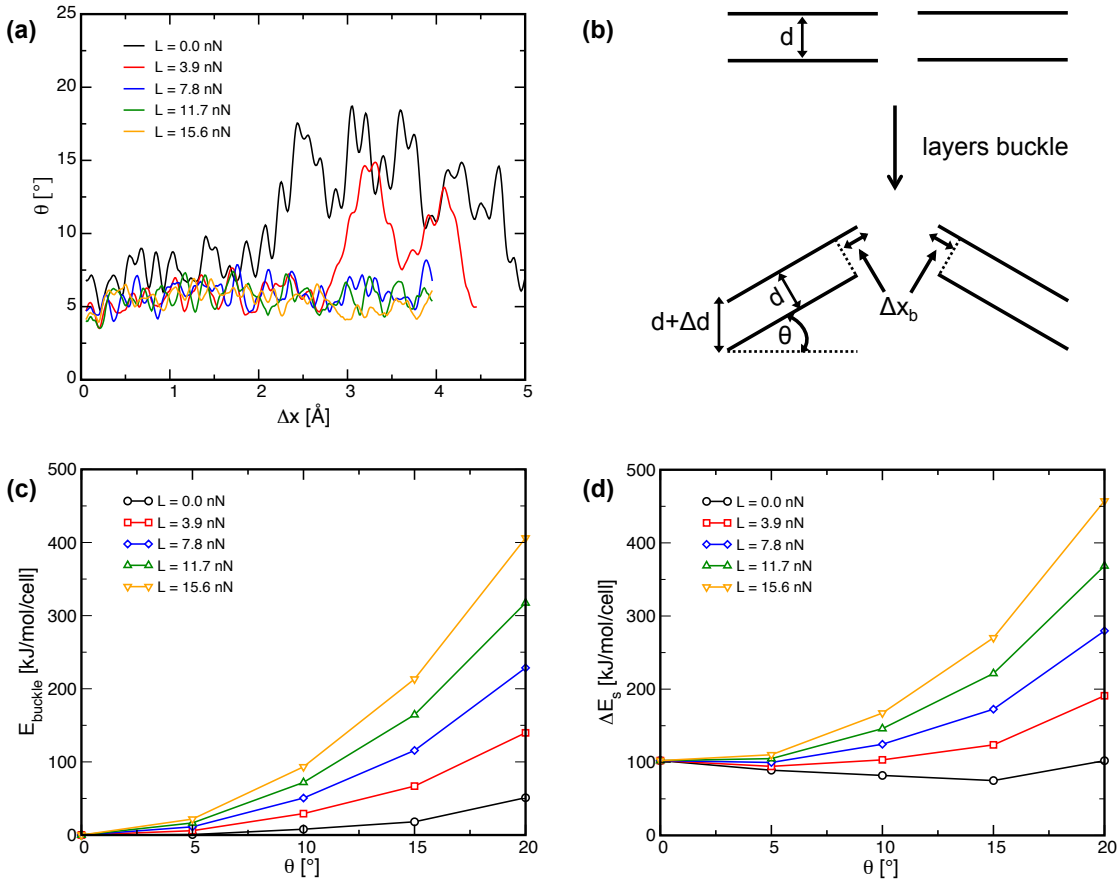

Figure 3.11. (a) Average angle, θ, between the normals to the rings in the system and the *z* direction versus Δ*x* for simulations performed with various normal loads. The data show that the layers buckle considerably during slip at the lowest two loads considered. (b) A schematic showing how the geometries of the layers are affected by buckling. The upper portion of the schematic illustrates two sets of parallel rings separated by a distance, *d*. Buckling causes one pair of rings to rotate through a positive angle and the other set to rotate through a negative angle. The rotation increases the thickness of the system by $\Delta z = N\Delta d$. In addition, rotation causes adjacent rings to move by an amount Δx_b relative to one another. Specifically, for the rings that rotate through a negative angle, the upper ring moves Δx_b relative to the bottom ring. Meanwhile, the upper ring moves a distance $-\Delta x_b$ relative to the lower ring for the pair of rings that rotate through a positive angle. (c) The change in energy, E_{buckle}, due to buckling the system by angle θ at different *L*. (d) The estimated slip barriers, E_s, obtained through Eq. (3.3) versus θ at different *L*.

The results presented in Section 3.4 for System **3** sheared in the absence of a normal load showed that the slip mechanism for this system involved the layers becoming buckled. The rotation of the monomers within the layers associated with the buckling process was found to allow adjacent pairs of strands of rings to move past one another in a stepwise manner during

slip, as opposed to requiring all strands to move past one another simultaneously. Analysis of the structures of the systems sheared under load showed that the buckled slip mechanism also occurred when L = 3.9 nN, but did not occur at higher L. This is evident from the data in Figure 3.11a, which show the average absolute value of the angle, θ, between the vertical (z) axis and the normal to each ring in the system. This normal is defined by the positions of the three nitrogen atoms in each ring. This value of θ is shown against the shear distance for one simulation performed at each L considered. The data for L = 0 and 3.9 nN show sharp increases in θ with increasing Δx to reach values between 10° and 20°, followed by sharp drops in θ at higher Δx. The sharp changes in θ correspond to the points at which the first and second strand of rings pass over one another as described in the previous section for the system simulated at L = 0 nN. Meanwhile, θ oscillated around 5° for the simulations performed at higher loads.

The buckled slip mechanism is evidently a lower energy process at low L than the competing process in which all pairs rings move past one another simultaneously. The advantage of the stepwise process becomes clear if the slip barrier, E_s, is assumed to be additive, i.e. $E_s = N_s E_s^1(\Delta x_s)$, where N_s is the number of pairs of rings that move past one another and $E_s^1(\Delta x)$ is the change in energy due to moving one pair of rings past one another a distance Δx along the slip direction from the equilibrium structure, and Δx_s is the value of Δx at which slip occurs. Essentially, the stepwise mechanism reduces N_s, which in turn reduces E_s. Of course a simple additive model neglects changes in energy associated with the change in structure due to the buckling process itself. The relevant structural changes associated with buckling are illustrated in Figure 3.11b. The upper portion of this figure illustrate two neighboring pairs of rings, which are arranged in a flat manner, i.e. θ = 0°, with the layers of rings separated by a distance d. At the point where slip occurs in this flat arrangement, each ring will have moved Δx_s

along the slip direction relative to its position in the equilibrium structure of the system. Buckling causes a given pair of rings to move relative to one another by an amount Δx_b as indicated in the bottom panel in Figure 3.11b. If one assumes that d remains constant during the buckling process, $\Delta x_b = d\tan\theta$. The forward motion of the upper ring in the leftmost pair of rings in the bottom panel in Figure 3.11b contributes to the slip process, but ultimately this pair of rings must undergo a relative movement of Δx_s for slip to occur. Meanwhile, the movement of the upper ring in the rightmost pair of rings in Figure 3.11 by an amount of $-\Delta x_b$ along the slip direction due to buckling allows this pair of rings to exist at a relative position of $\Delta x = \Delta x_s - \Delta x_b$ when the pair of rings of the left hand side of the figure are at a relative position of Δx_s. As such, the pair of rings on the left side of the figure will have an energy of $E_s^1(\Delta x_s)$, whereas the energy of the set of rings on the right of the figure will be $E_s^1(\Delta x_s - \Delta x_b)$. In addition, buckling the layers causes a change in height of $\Delta z = N_l d\sec\theta$, where N_l is the number of layers and once again it is assumed that d is a constant. As such, work in the amount of $L\Delta z$ will be performed when buckling occurs in the presence of a load. Note that this definition of Δz is only correct for a system that is infinitely repeated along the z direction, as is the case for the FPMD simulations considered here. In a system of finite thickness, a contribution of $l\sin\theta$ would have to be added to the definition of Δz, where l corresponds to the length of one ring along the slip direction. Finally, there is a change in energy, E_{buckle}^1, associated with buckling a layer in the system from its equilibrium structure.

Altogether, the mechanism illustrated in Figure 3.11b leads to an estimated slip barrier of:

$$E_s(\theta, L) = 2E_s^1(\Delta x_s) + 2E_s^1(\Delta x_s - \Delta x_b) + 2E_{buckle}^1(\theta) + L\Delta z \qquad \text{(Eq. 3.3)}$$

where the factors of 2 in front of the $E_s^1(\Delta x_s)$ and $E_s^1(\Delta x_s - \Delta x_b)$ appear because the simulation cell contains two pairs of rings in each strand associated with these terms. The values of Δx_s and $E_s^1(\Delta x)$ were obtained by performing potential energy surface scans on the model of System **3** described above in which the upper layer of rings was moved along the slip direction by a distance Δx relative to the lower set of rings followed by a constrained optimization of the structure in which the atomic positions along directions orthogonal to the slip direction and the z component of the **c** lattice vector were allowed to relax with L = 0.0 nN. This process led to a value of Δx_s = 1.98 Å and the values of $E_s^1(\Delta x)$ at other values of Δx entering Eq. (3.3). The values of Δx and Δz were obtained using the equations provided above in conjunction with the value of d in Table 1. These results were then used to estimate the energetics associated with the slip process at different θ and L. The values of E_{buckle}^1 were obtained by rotating the rings in a single layer of System **3** by θ and allowing the atoms to relax while keeping θ constant.

The changes in energy associated with buckling, $E_{buckle}(\theta, L) = 2E_{buckle}^1(\theta) + L\Delta z$, at various L are plotted in Figure 3.11c versus θ. The data show that buckling the layers by small angles incurs relatively small energetic penalties, with E_{buckle} below 25 kJ/mol·cell for θ = 5° at all L. Meanwhile, E_{buckle} increases significantly at higher θ for higher values of L, which is a result of the work that must be performed to change the thickness of the system in the presence of a normal load. While the approximate nature of this analysis renders the values in Figure 3.11c semi-quantitative at best, they are consistent with the results of the FPMD simulations, which showed that System **3** adopted values of $\theta \sim 5°$ before slip occurred at all L.

The estimated barriers to slip at different θ and L given by Eq. (3.3) are shown in Figure 3.11d. The barrier at $\theta = 0°$ corresponds to the barrier to slip through a mechanism in which the layers remain completely flat and all pairs of rings move past one another simultaneously. Meanwhile, the values of E_s at higher θ correspond to a slip mechanism involving the stepwise movement of the pairs of rings past one another. As noted above, these data were obtained using structures with L = 0.0 nN, and hence the barrier when $\theta = 0°$ is the same for all systems. This is clearly an approximation, since changes in the thickness of the system during shear will lead to load-dependent contributions to the slip barrier at non-zero L. Nonetheless, the changes in E_s with θ for a given L in Figure 3.11d provide qualitative insights into the ability of System **3** to undergo a stepwise slip mechanism at different L. The data in Figure 3.11d show that buckling the system reduces E_s for θ up to 15° when L = 0.0 nN. Similarly, buckling the system to approximately 10° leads to lower values of E_s than that associated with the mechanism in which the rings remain completely flat. At higher L, the values of E_s for a stepwise mechanism with $\theta =$ 5° are slightly higher than E_s with $\theta = 0°$, which suggests that the stepwise slip mechanism does not occur at these higher values of L. Overall, these results are qualitatively consistent with the results of the FPMD simulations. While this only a semi-quantitative analysis, it clearly demonstrates that the buckled slip mechanism can reduce slip barriers at low L, whereas the application of higher L suppresses this slip mechanism due to the work that must be performed to change the thickness of the system in the presence of L. It is noted that the conclusion that the buckled slip mechanism is preferred at low loads is based on considerations of potential energies that are independent of sliding velocity, and thus this mechanism should continue to be observed at the lower sliding velocities that are likely encountered in real-world scenarios. This was

examined by performing additional simulations of System **3** in the absence of an applied load at sliding velocities of 0.2 and 0.5 Å/ps.

---

(1) Glidewell, C.; Low, J. N.; Melguizo, M.; Quesada, A. 4-Amino-2,6-Dimethoxypyrimidine: Hydrogen-Bonded Sheets of R 2 2 (8) and R 6 6 (28) Rings, Reinforced by an Aromatic Π–π-Stacking Interaction. *Acta Crystallogr. Sect. C Cryst. Struct. Commun.* **2003**, *59*, o202–o204.

(2) Uemura, S.; Aono, M.; Komatsu, T.; Kunitake, M. Two-Dimensional Self-Assembled Structures of Melamine and Melem at the Aqueous Solution-Au(111) Interface. *Langmuir* **2011**, *27*, 1336–1340.

(3) Wasio, N. a; Quardokus, R. C.; Forrest, R. P.; Lent, C. S.; Corcelli, S. a; Christie, J. a; Henderson, K. W.; Kandel, S. A. Self-Assembly of Hydrogen-Bonded Two-Dimensional Quasicrystals. *Nature* **2014**, *507*, 86–89.

(4) MacGillivray, L. R. Organic Synthesis in the Solid State via Hydrogen-Bond-Driven Self-Assembly. *J. Org. Chem.* **2008**, *73*, 3311–3317.

(5) Bowden, N. Self-Assembly of Mesoscale Objects into Ordered Two-Dimensional Arrays. *Science (80-.).* **1997**, *276*, 233–235.

(6) Prior, T. J.; Armstrong, J. a.; Benoit, D. M.; Marshall, K. L. The Structure of the Melamine–cyanuric Acid Co-Crystal. *CrystEngComm* **2013**, *15*, 5838.

(7) Erbaş, A.; Horinek, D.; Netz, R. R. Viscous Friction of Hydrogen-Bonded Matter. *J. Am. Chem. Soc.* **2012**, *134*, 623–630.

(8) Yue, D. C.; Ma, T. B.; Hu, Y. Z.; Yeon, J.; Van Duin, A. C. T.; Wang, H.; Luo, J. Tribochemistry of Phosphoric Acid Sheared between Quartz Surfaces: A Reactive Molecular Dynamics Study. *J. Phys. Chem. C* **2013**, *117*, 25604–25614.

(9) Scharf, T. W.; Prasad, S. V. Solid Lubricants: A Review. *J. Mater. Sci.* **2012**, *48*, 511–531.

(10) Zhang, J.; Chen, P.; Yuan, B.; Ji, W.; Cheng, Z.; Qiu, X. Real-Space Identification of Intermolecular Bonding with Atomic Force Microscopy. *Science* **2013**, *342*, 611–614.

(11) Giannozzi, P.; Baroni, S.; Bonini, N.; Calandra, M.; Car, R.; Cavazzoni, C.; Ceresoli, D.; Chiarotti, G. L.; Cococcioni, M.; Dabo, I.; et al. QUANTUM ESPRESSO: A Modular and Open-Source Software Project for Quantum Simulations of Materials. *J. Phys. Condens. Matter* **2009**, *21*, 395502.

(12) Kohn, W.; Sham, L. J. Self-Consistent Equations Including Exchange and Correlation Effects. *Phys. Rev.* **1965**, *140,* A1133-A1138.

(13) Hohenberg, P.; Kohn, W. Inhomogeneous Electron Gas. *Phys. Rev.* **1964**, *136*, B864–B871.

(14) Perdew, J.; Burke, K.; Ernzerhof, M. Generalized Gradient Approximation Made Simple. *Phys. Rev. Lett.* **1996**, *77*, 3865–3868.

(15) Grimme, S.; Antony, J.; Ehrlich, S.; Krieg, H. A Consistent and Accurate Ab Initio Parametrization of Density Functional Dispersion Correction (DFT-D) for the 94 Elements H-Pu. *J. Chem. Phys.* **2010**, *132*, 154104.

(16) Grimme, S. Semiempirical GGA-Type Density Functional Constructed with a Long-Range Dispersion Correction. *J. Comput. Chem.* **2006**, *27*, 1787–1799.

(17) Ireta, J.; Neugebauer, J.; Scheffler, M. On the Accuracy of DFT for Describing Hydrogen Bonds: Dependence on the Bond Directionality. *J. Phys. Chem. A* **2004**, *108*, 5692–5698.

(18) Grimme, S.; Antony, J.; Schwabe, T.; Mück-Lichtenfeld, C. Density Functional Theory with Dispersion Corrections for Supramolecular Structures, Aggregates, and Complexes of (bio)organic Molecules. *Org. Biomol. Chem.* **2007**, *5*, 741–758.

(19) Blöchl, P. E. Projector Augmented-Wave Method. *Phys. Rev. B* **1994**, *50*, 17953–17979.

(20) Bernasconi, M.; Chiarotti, G. L.; Focher, P.; Scandolo, S.; Tosatti, E.; Parrinello, M. First-Principle-Constant Pressure Molecular Dynamics. *J. Phys. Chem. Solids* **1995**, *56*, 501–505.

(21) Andersen, H. . Molecular Dynamics Simulations at Constant Pressure And/or Temperature. *J. Chem. Phys.* **1980**, *72*, 2384–2393.

(22) Lees, a W.; Edwards, S. F. The Computer Study of Transport Processes under Extreme Conditions. *J. Phys. C Solid State Phys.* **1972**, *5*, 1921–1928.

(23) Parrinello, M.; Rahman, A.; Parrinello M, R. A. Crystal Structure and Pair Potentials: A Molecular_Dynamics Study. *Phys. Rev. Lett.* **1980**, *45*, 1196–1199.

(24) Carkner, C. J.; Haw, S. M.; Mosey, N. J. Effect of Adhesive Interactions on Static Friction at the Atomic Scale. *Phys. Rev. Lett.* **2010**, *105*, 056102.

(25) Gao, J.; Luedtke, W. D.; Gourdon, D.; Ruths, M.; Israelachvili, J. N.; Landman, U. Frictional Forces and Amontons' Law: From the Molecular to the Macroscopic Scale. *J. Phys. Chem. B* **2004**, *108*, 3410–3425.

(26) Derjaguin, B. V. Mechanical Properties of the Boundary Lubrication Layer. *Wear* **1988**, *128*, 19–27.

(27) Briscoe, B. J.; Evans, D. C. The Shear Properties of Langmuir-Blodgett Layers. *Proc. R. Soc. A* **1982**, *380*, 389–407.

(28) Abrahamson, J. The Surface Energies of Graphite. *Carbon*, 1973, *11*, 337–362.

(29) Gaur, A. P. S.; Sahoo, S.; Ahmadi, M.; Dash, S. P.; Guinel, M. J. F.; Katiyar, R. S. Surface Energy Engineering for Tunable Wettability through Controlled Synthesis of MoS2. *Nano Lett.* **2014**, *14*, 4314–4321.

(30) Steiner, T. The Hydrogen Bond in the Solid State. *Angew. Chem. Int. Ed.* **2002**, *41*, 49–76.

(31) L**ö**wdin, P.-O. On the Non-Orthogonality Problem. *Adv. Quantum Chem.* **1970**, *5*, 185–199.

(32) Löwdin, P.-O. On the Non-Orthogonality Problem Connected with the Use of Atomic Wave Functions in the Theory of Molecules and Crystals. *J. Chem. Phys.* **1950**, *18*, 365–375.

(33) Zartman, G. D.; Liu, H.; Akdim, B.; Pachter, R.; Heinz, H. Nanoscale Tensile, Shear, and Failure Properties of Layered Silicates as a Function of Cation Density and Stress. *J. Phys. Chem. C* **2010**, *114*, 1763–1772.

(34) *CRC Handbook of Chemistry and Physics*; 95th ed.; CRC Press: Boca, Raton, FL, 2014; p. 2693.

(35) Atkins, P. *Inorganic Chemistry*. W.H. Freeman: New York, **2006**.

(36) Donnet, C.; Martin, J. M.; Le Mogne, T.; Belin, M. The Origin of Super-Low Friction Coefficient of MoS2 Coatings in Various Environments. *Tribol. Ser.* **1994**, *27*, 277–284.

(37) Saito, T.; Honda, F. Chemical Contribution to Friction Behavior of Sintered Hexagonal Boron Nitride in Water. *Wear* **2000**, *237*, 253–260.

Chapter 4: Conclusion

Understanding the response of different materials to tribological conditions can aid in the development of new and improved lubricants. The goal of this thesis was to use static QC calculations and FPMD simulations to examine the behavior of model 2D hydrogen-bonded networks in response to applied shear strains with the goal of assessing whether such systems may be useful as lubricants. The systems considered for this work were designed to form sheets that could be stacked in a manner analogous to that in which layers of graphene are stacked in graphite. The rationale behind the design of these systems relies heavily on the fact that like graphite, the weak interactions between the layers could allow the sheets to slide past one another with little effort and may lead to low shear stresses and in turn low friction forces. Unlike graphene sheets, however, these hydrogen-bonded components that hold together each sheet are much more flexible than the rigid covalent or ionic bond counterpart. The hydrogen-bonded nature of the sheets offers the potential for them to reform after stress-induced disruptions in the structure. The ability of the sheets to reform may represent an advantage over solid lubricants composed of covalently and/or ionically bonded sheets, e.g. graphite or MoS_2, which can undergo irreversible changes in structure.

The design of model systems illustrates the challenges associated with developing 2D hydrogen-sheets. In particular, the placement and mobility of HB donors and acceptors is key to the formation of the sheets. The placement of these groups is important in the context of ensuring that there are a sufficient number of HBs between molecular units to form well-structured layers. Meanwhile, restricting the ability of the HB donors and acceptors to point in directions that are not parallel to the layers is key to ensuring that the HB interactions are directed between molecules in the same layers, which leads to robust layers, as opposed to directed between

layers, which causes the systems to reorganize. The systems considered for this study were examined because geometry optimizations indicated that they can form layered structures of the type at the focus of this work. However, systems similar to those considered in this work have been found to form layered structures. For example, combining melamine with the molecules forming System **3** and other small molecules yields 2D hydrogen-bonded structures.[1,2]

Static QC calculations showed that all three systems considered had low interlayer interaction strengths, comparable to those of systems like graphite and MoS_2, which suggested that these systems may have low shear strengths. Meanwhile, the systems had very different HB energies, with these energies increasing as **2** < **3** < **1**. FPMD simulations and static quantum chemical calculations of **1** indicated that the N-H interactions were sufficiently strong to induce proton transfer processes that caused System **1** to exist preferentially as **1b**.

The systems were sheared in the absence of an applied load to examine their responses to tribological conditions. The results indicated that Systems **1** and **2** are unlikely to be effective lubricants. System **1** exhibited a high stiffness and ultimately underwent a reaction that led to the formation of C-C bonds between molecules in adjacent layers. System **2** underwent a slip process with a relatively low shear strength (~1.5 GPa). After slip occurred, this system underwent a significant structural reorganization progress that led to the loss of the layered structure and large increases in τ. This behavior is undesirable from the standpoint of lubrication and occurred as a result of changes in the directions in which the HBs pointed. This reorientation of the HBs was possible because the HBs in this system are relatively weak and localized to small regions of the system. The weak nature of these HBs allows them to dissociate, whereas the localized nature of the HBs within the system leads to situations in which a large number of interlayer HBs can be formed simultaneously.

The results of the FPMD simulations performed over a wide range of loads indicated that System **3** may be an effective lubricant, with this system exhibiting low friction forces, a low friction coefficient, and the ability to retain a layered structure. The low friction forces and coefficients arise from the weak interlayer interactions strengths. Meanwhile, the ability of System **3** to retain its structure stemmed from the fact that the HBs were sufficiently strong to discourage their dissociation during slip, as evidenced by data in Figure 3.8, yet sufficiently weak to discourage the types of proton transfer reactions that were problematic for System **1**. In addition, the HBs were symmetrically distributed around each molecule in System **3**, as opposed to being present in fairly localized regions of space as in System **2**, which also discourages the rotation of the molecules forming the system to permit the formation of HBs between layers.

The FPMD simulations showed that System **3** underwent a slip mechanism in which the layers buckled at low L, and remained flat at higher L. Analysis of the energetics associated with slip showed that the buckled mechanism allows the rings in the system to move past one another in a stepwise manner, which leads to a lower potential energy barrier than a competing process in which all rings move past one another simultaneously. Meanwhile, the energetic cost associated with increasing the thickness of the system against a normal load due to buckling renders the buckled mechanism unfavorable at higher L. The ability of 2D hydrogen-bonded systems to undergo this buckled mechanism at low loads may represent an advantage over covalently-bonded layers in the context of lubrication because covalently-bonded layers cannot easily buckle.

Overall, the results of this thesis indicate that 2D hydrogen bonded systems may be effective lubricants provided that layers can be formed and retained. The factors involved in achieving this are the positions, strengths, and directional flexibilities of the HBs. In particular, it

is advantageous for the HBs to be arranged symmetrically around the molecules forming the layers and the HBs should be sufficiently strong to inhibit the decomposition of the layers, but sufficiently weak to discourage proton transfer reactions. In addition, the groups selected as HB donors and acceptors should be able to be restricted to lie within the planes corresponding to the layers in the system to prevent the formation of HBs between layers.

The present work focused on molecular units consisting of one ring or two fused rings. While systems like these have been found to form 2D hydrogen-bonded networks[1,2], it may be interesting in the context of lubrication to consider components consisting of larger planar molecules with HB donors and acceptors bonded or replacing the outer atoms of the rings. Layers formed from such species will possess low interlayer strengths, leading to low friction forces, and possess the structural robustness and reversibility offered by the HBs, yet the larger surface areas of the monomers may facilitate the alignment of the layers parallel to surfaces in contacts. In fact systems like these based on melamine and melem have been reported recently.[2]

Future work may consist of expanding some of the more promising structures like System **3** and further studying them through the use of force fields, allowing one to simulation a more realistic size of system (thousands of atom) and in a much less demanding time scale. As well, using force fields that allow for a more generous atom size capacity, would give one the option of studying preexisting experimental 2D hydrogen-bonded systems and observing their shear strengths to see if they too could be suitable as lubricants. If the results of such calculations indicate that 2D HB networks may be useful as lubricants, additional experimental work would be required to assess whether this conclusion holds true under conditions experienced within actual sliding contacts.

(1) Prior, T. J.; Armstrong, J. A.; Benoit, D. M.; Marshall, K. L. The Structure of the Melamine–cyanuric Acid Co-Crystal. *CrystEngComm* **2013**, *15*, 5838.

(2) Uemura, S.; Aono, M.; Komatsu, T.; Kunitake, M. Two-Dimensional Self-Assembled Structures of Melamine and Melem at the Aqueous Solution-Au(111) Interface. *Langmuir* **2011**, *27*, 1336–1340.